AD-A136 980 PREDICTING THE ONSET OF TURBULENCE IN THE PRESENCE OF A PRESSURE GRADIENT(U) AIR FORCE INST OF TECH WRIGHT-PATTERSON AFB OH SCHOOL OF ENGINEERING 1/1

UNCLASSIFIED R D CHARLES DEC 83 AFIT/GAE/AA/83D-4 F/G 20/4 NL

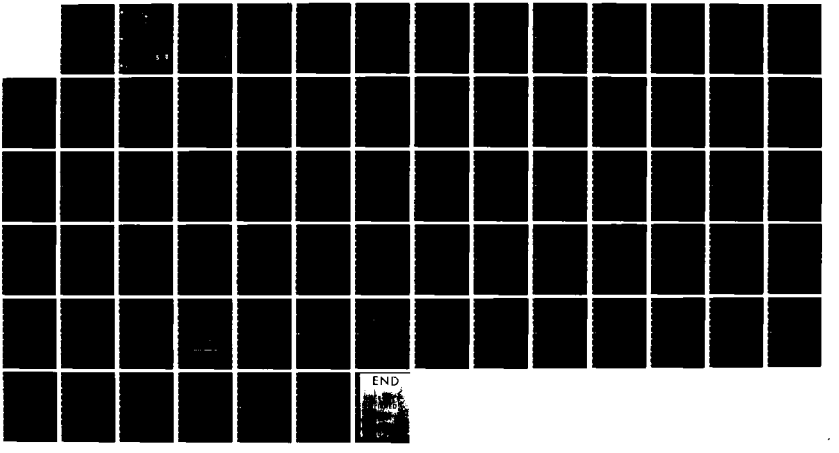

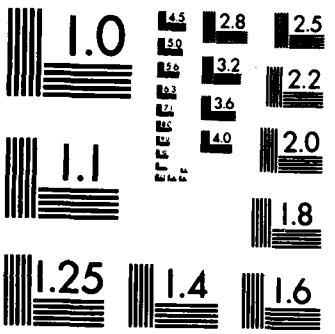

PREDICTING THE ONSET OF TURBULENCE IN THE PRESENCE OF A PRESSURE GRADIENT

THESIS

Richard D. Charles

AFIT/GAE/AA/83D-[illegible] 2Lt USAF

DEPARTMENT OF THE AIR FORCE
AIR UNIVERSITY
AIR FORCE INSTITUTE OF TECHNOLOGY

Wright-Patterson Air Force Base, Ohio

AFIT/GAE/AA/83D-4

PREDICTING THE ONSET OF TURBULENCE IN THE PRESENCE OF A PRESSURE GRADIENT

THESIS

Richard D. Charles
AFIT/GAE/AA/83D-4 2LT. USAF

AFIT/GAE/AA/83D-4

PREDICTING THE ONSET OF TURBULENCE IN THE PRESENCE OF A PRESSURE GRADIENT

THESIS

Presented to the Faculty of the School of Engineering of
the Institute of Technology
Air University
In Partial Fulfillment of the
Requirements for the Degree of
Master of Science

By

RICHARD D. CHARLES, B.S.M.E.
2LT. USAF
GRADUATE AERONAUTICAL ENGINEERING

DECEMBER 1983

Acknowledgements

The nature of this thesis was similar to the working of a pictureless jigsaw puzzle. My great thanks go to my advisor, Major E. Jumper, who was repeatedly helpful in suggesting ways to find the missing pieces of the theory presented herein. Further, Dr. J. Hitchcock was a great aid in my being able to adapt external flow relationships to internal flow applications, thereby supplying more pieces of the puzzle. And finally, my deep thanks go to the AFIT Library staff and in particular, Mrs. Linda Stoddard, without whose help, and ability to locate elusive foreign journals, there would have been no raw material to fashion into this thesis.

Richard D. Charles

Contents

Contents (con't)

List of Symbols

$C = C_r + iC_i = \beta/\alpha$

C_i = amplification (or damping) factor

C_r = wave propagation speed of disturbance

d,D = diameter

g = acceleration due to gravity

h = channel width

$i = \sqrt{-1}$

l,L = length

m = flow exponent

P = pressure (force per unit area)

r,R = radius

R,Re = $(UL/\nu$ or $\bar{U}d/\nu$ or $U\delta/\nu$ = Reynolds number

R_{crit} = critical Reynolds number

R_{trans} = transition Reynolds number

$\Delta R = R_{trans} - R_{crit}$

$\bar{U}$ = mean velocity (in pipe)

$U_m = U_o x^m$ = velocity in potential flow

U = maximum velocity

U_∞ = free-stream velocity

u,v,w = veloctiy components

u',v',w' = velocity components of disturbance

List of Symbols (con't)

$\bar{u}$ = temporal mean velocity

$U(y)$ = boundary-layer velocity distribution

x,y,z = cartesian coordinates

x = streamwise coordinate

y,z = coordinates normal to flow direction

α = wave-number of disturbance

$\beta = \beta_r + i\beta_i$

β_i = amplification (or damping) factor

β_r = circular frequency of disturbance

δ = boundary-layer thickness

δ_1, δ^* = displacement thickness

δ_2, θ = momentum thickness

$\eta = y/\delta$ = non-dimensional displacement

λ = momentum thickness Pohlhausen parameter

Λ = boundary-layer thickness Pohlhausen parameter

μ = viscosity

ν = kinematic viscosity

ρ = fluid density

$\phi(y)$ = amplitude of stream function of disturbance

List of Figures

List of Tables

Abstract

An analytical study is presented regarding the determination of a pressure gradient dependent criterion for flow transition from laminar to turbulent flow. The results obtained were derived from two parallel approaches to 'ow stability; one of wave-dependent stability and the oth of vorticity-dependent stability. In both cases, one a variable transition Reynolds number dependent upor .ie ambient pressure gradient and the other one of a constant transition Reynolds number based on the boundary-layer displacement thickness, the prediction results were either as good or better than those from available prediction methods. In addition these two criteria were used to predict transition locations on a NACA 0018 airfoil, again with favorable results.

I. Introduction

Discussion

The development of an understanding of the mechanism or mechanisms responsible for the transition from laminar to turbulent flow is one of the most unknown areas in the field of fluid mechanics today. Rather than being dependent upon one flow condition or parameter the actions of flow transition is seen to be a function of many different flow factors that are not necessarily independent of one another. Some of these are: the roughness of the flow passage walls; heating or cooling of the passage walls; obstructions in the flow field; blowing or suction at the passage walls; mass transfer or chemical reaction with the passage walls; pressure pulses (noise) in the flow; deformable wall geometry; and, ambient pressure gradients in the flow (Ref. 1). One of the major problems in either an experimental or analytic treatment of this subject is the difficulty in isolating the effect of the variation of one flow parameter while keeping the others constant. This problem is due to both the technical difficulties encountered in monitoring and controlling the other parameters and to the functional interdependence of these parameters which results in large data scatters in similar investigations and inhibits comprehensive studies of flow transition. These complications have resulted in

significant obstacles in the theoretical study of flow transition and have limited the experimental data to a small, specialized body. The many parameters used to characterize the flow take a wide variety of functional forms which also tend to defy correlation into a comprehensive picture.

An additional barrier to fluid transition study is that not only are the factors affecting transition variable in their effect upon transition and related to each other in a complicated manner, but transition, and subsequently transition data, has not been uniquely defined. Although there exist universally accepted concepts for laminar flow and turbulent flow, the transition of a flow has been variously reported in terms of: the start of transition (the appearance of turbulent spots); the end of transition (the flow consisting of a variably-defined level of turbulence); or, a region of transition that lies between fully-laminar flow and fully-turbulent flow and contains the two previously mentioned boundaries. Finally, most theoretical studies of this field, both analytic and numerical, do not deal with transition at all but with flow instability where an unstable flow is defined as a flow which contains Tollmein-Schlichting waves of such frequencies and wavelengths that their amplitudes will tend to magnify as a function of time and will subsequently cause the flow transition to turbulence.

Problem Statement

With the above limitations taken into consideration, this study focused on only the effect of an ambient pressure gradient in the flow on the mechanism of transition. An empirical prediction method based on a transition Reynolds number, based on fluid boundary-layer momentum thickness, was developed by Kays and Crawford (Ref. 2) that yielded a single value of 360 for a flow regardless of the history of the flow boundary layer. Hermann Schlichting (Ref. 1), conversely, reported a theoretical dependence of fluid instability on the presence of a pressure gradient where he used a critical Reynolds number based on the fluid boundary-layer displacement thickness. This study sought to develop a prediction method that blended these two ideas into a single criterion (i.e., encompass both the momentum interaction of the boundary layer and the influence of the presence of a flow pressure gradient).

II. Background

Stability Theory

The origins of flow stability theory are derived from an attempt by fluid mechanicists to explain flow transitions from first principles. This theory is based directly upon the incompressible, three-dimensional Navier-Stokes equations with the assumption of one-dimensional perturbation velocities. With the use of perturbation theory, the assumption of small amplitude disturbances, and the retention of only the linear perturbation terms, the Navier-Stokes equations are transformed into what is commonly known as the Orr-Sommerfeld equation. A full derivation of the Orr-Sommerfeld equation, based in part upon the treatment of Hunt (Ref. 3) and in part upon that of Schlichting (Ref. 1) is given in Appendix A. The usual form of the equation is:

$$(\bar{u}-c)(\phi'' - \alpha^2\phi) - \bar{u}''\phi = \frac{-i}{\alpha R}(\phi'' - 2\alpha^2\phi'' + \alpha^4\phi) \qquad (1)$$

where

$\bar{u}$ = boundary layer velocity profile

c = complex wave speed

ϕ = wave amplitude

α = wave number

$i = \sqrt{-1}$

R = Reynolds number (usually based upon edge velocity and displacement thickness)

and all variables are nondimensional with the primes denoting derivatives with respect to the coordinate normal to the mean flow direction.

The Orr-Sommerfeld equation represents a complex, fourth-order homogeneous ordinary differential equation in $\emptyset$, yet with both $\bar{u}$ and $\emptyset$ being functions of the normal coordinate and due to the fact that (C, α, R) represent a related family of parameters, there is no closed-form solution to this equation. Thus, the main tool of flow stability has no known exact solution. Common approximate analytic solutions use asymptotic approximations that involve recursive Hankel functions of order 1/3, such as Lin's method (Ref. 4). Existing computer-aided numerical solutions as a rule either use eigen-value "shooting methods" (Ref 5) or expand the equation in terms of orthogonal polynomials, such as Chebyshev polynomials (Ref. 6), and use successive-guess and recursive relationships among the polynomials to achieve approximate solutions to the Orr-Sommerfield equation.

The usual method of presenting these stability results is in the form of a neutral stability curve (see Fig. 1). In this plot, the curve represents the variation of wave number as a function of Reynolds number. The points on the curve represent Reynolds numbers and wavenumber combinations

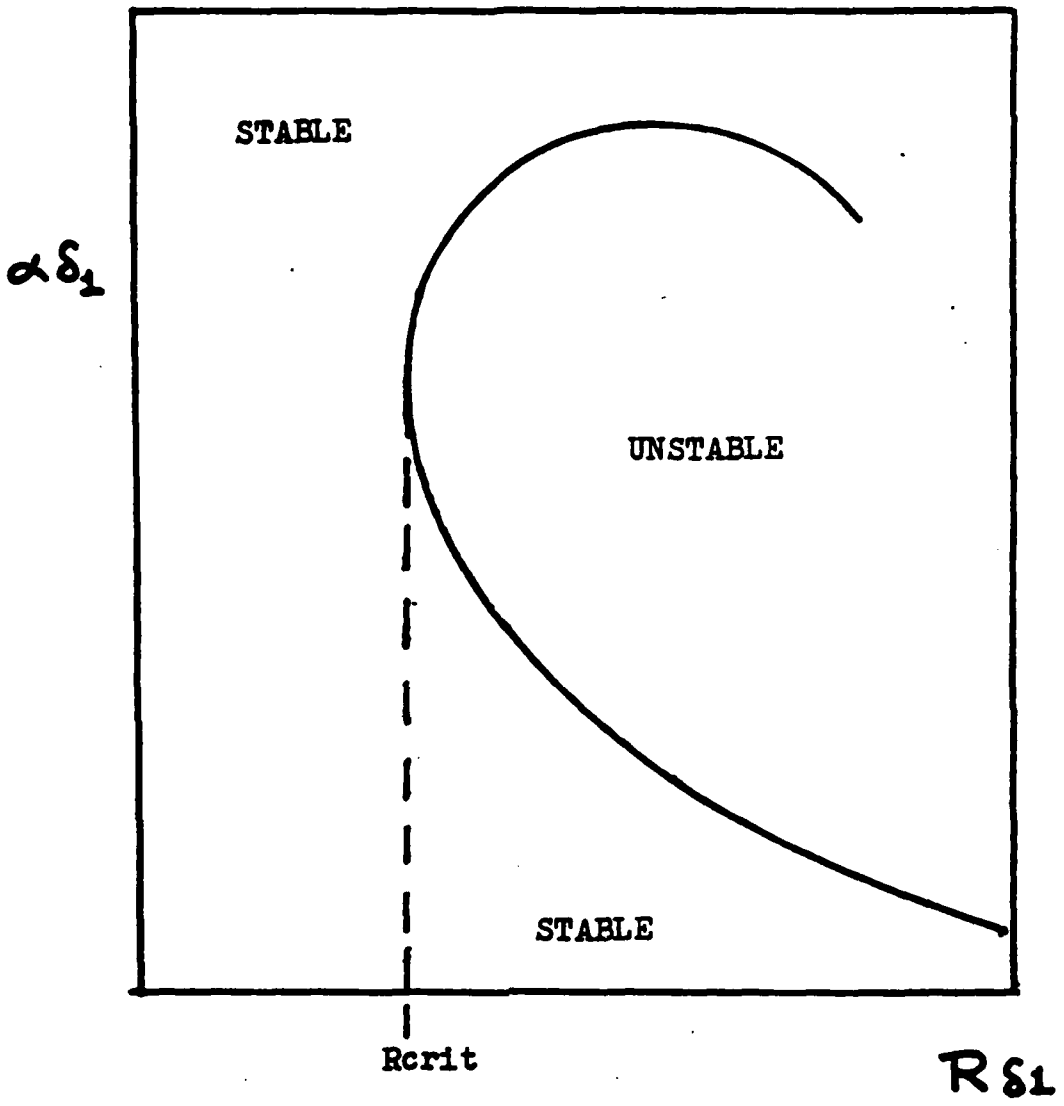

Fig 1 A Typical Stability Diagram.

which do not tend to be amplified or dampened temporally for the associated waves. The region outside of the curve represents those combinations of wavenumber and Reynolds number for which disturbances tend to damp-out and the region inside the curve represents those combinations for which disturbances tend to be amplified and for which the flow is said to be unstable. The Reynolds number below which no value of wavenumber will yield unstable flow is said to be the critical Reynolds number and is the minimum value of the Reynolds number on the curve. Due to the approximate nature of the existing solutions there is a considerable variation of determined Rcrit values as can be seen in Fig. 2 which is from a compilation by van Ingen (Ref. 7) where Rcrit varies from 321 to 680. With this large variation in mind, stability theory results are treated warily and are considered as approximate only.

Transition Versus Instability

Stability theory, though it is derived from first principles through the Navier-Stokes equations, is in fact quite limited when true transition is considered. Besides the approximate nature of the Orr-Sommerfeld equation solution which does not yield unique values for any one flow situation treated by stability theory, most common flows tend to violate one or more of the basic assumptions used to derive the theory. Some of these violations are: velocity components nonparallel to the mean flow direction that tend

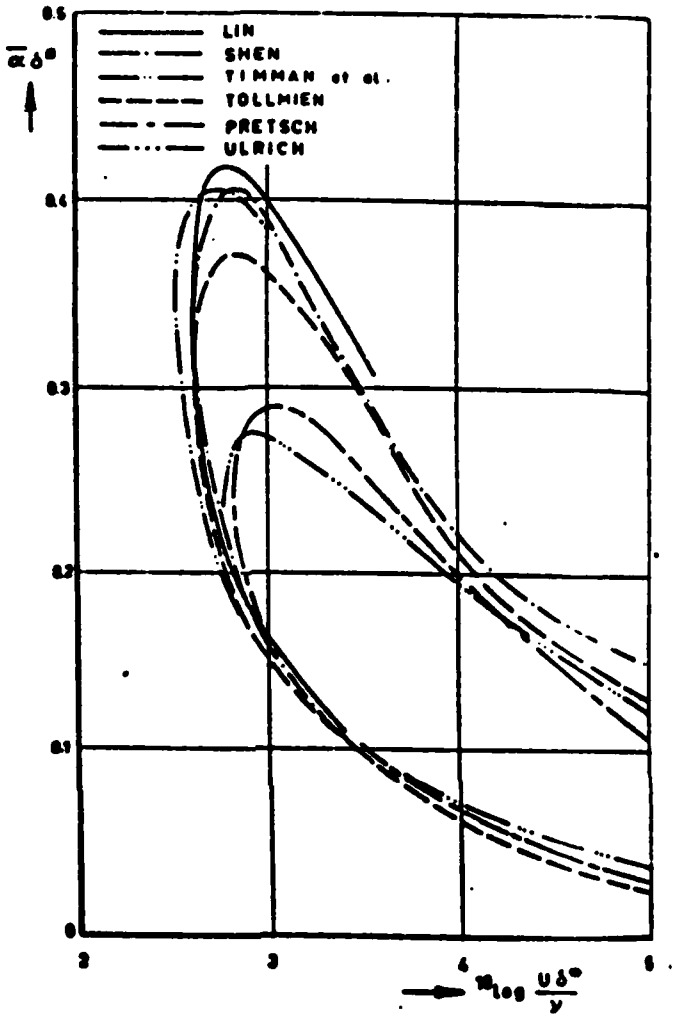

Fig 2 Neutral Stability Curves for Flat Plate Flow with Zero Pressure Gradient from Different Sources. (Ref.7)

to make the flow unstable at lower Reynolds numbers; nonlinearity of the perturbation velocity components that tend to invalidate the linearized theory used to derive the Orr-Sommerfeld equation; dependence of the mean flow velocity on its streamwise coordinate that is neglected in stability theory derivations and adds another degree of complexity to the flow situation; and, large amplitude disturbances that are observed just prior to transition that are considered infinitesmal in magnitude for stability theory. Even with these severe limitations of stability theory, Rcrit is always less than Rtrans for a given flow case and thus provides a conservative criterion for transition. Furthermore, the behavior of Rcrit from one flow case to another tends to follow the same trends that Rtrans does, yielding a characteristic, if not exact, criterion for flow transition.

The fundamental basis of flow stability theory is that flow instability, and thus flow transition, is dependent upon the behavior of the amplification or dampening of the Tollmein-Schlichting waves present in the flow. A mechanism that does not depend on this type of wave action yet could plausibly play an equal if not greater role in flow transition would be a welcome addition to transition theory if it could be seen to have a firm foundation in first principles and also not to have many of the limitations of wave-theory. Such an approach which was based on "vorticity stability" was investigated in this study with favorable results.

III. Theory Development

The determination of a pressure gradient criterion for flow stability, and by allusion transition, required the knowledge of the values of Λ(Pohlhausen velocity profile shape parameter), δ (boundary layer thickness), $\delta 1$ (displacement thickness),and $\delta 2$ (momentum thickness) for each flow case in addition to the value of Rcrit. This was due to the fact that various sources based their cited values of Rcrit or Rtrans on either $\delta 1$ or $\delta 2$, or in the case of internal flow, Dh (hydraulic diameter) which could be related physically to for fully-developed internal flows.

Pressure Gradient Parameter

The pressure gradient parameter that was used throughout this study was Pohlhausen's shape factor based on boundary layer thickness, Λ , or a modified form commonly used which is based on momentum thickness, λ . The normal Pohlhausen parameter is defined as

$$\Lambda = \frac{\delta^2}{\nu} \frac{dUm}{dx} \qquad (2)$$

where Um = Um(x), and in the case of the wedge family, Um is of the form, $Um = Uox^m$, with Uo being a constant and x is the streamwise coordinate. λ is defined similarly as

$$\lambda = \frac{\delta_2^2}{\nu} \frac{dUm}{dx} \tag{3}$$

For the flow cases which were considered here, the flow was attached laminar flow, i.e. instability and transition occured before flow separation from the boundary wall. In the case of external flow, Bernoulli's equation for along a streamline outside the boundary layer is given as

$$\frac{dP}{dx} = -\rho Um \frac{dUm}{dx} \tag{4}$$

and this can be used with equation (1) to denote Λ and λ as pressure gradient parameters of the form:

$$\Lambda = \frac{-\delta^2}{\mu Um} \left(\frac{dP}{dx}\right) \tag{5}$$

$$\lambda = \frac{-(\delta_2)2}{\mu Um} \left(\frac{dP}{dx}\right) \tag{6}$$

This rendering of as a measure of the magnitude and typeof pressure gradient (Λ positive denoting a streamwise pressure drop, or favorable pressure gradient, etc.) was very convenient for the flat plate cases studied due to the common treatment (Ref. 1) of the boundary layer profile as a polynomial in Λ. Here, the velocity profile was of the form:

$$u(\eta) = Um\ -(2\eta-2\eta^3+\eta^4) + \frac{\Lambda}{6}(\eta-3\eta^2+3\eta^3-\eta^4) \qquad (7)$$

where η is a nondimensional coordinate to the flow commonly denoted as $\eta = y/\delta$. With the variation of Λ, different profiles of the nondimensional (corresponding to $u(\eta)/Um$) in equation (1)) were obtained by Schlichting (Ref. 1), et. al., that yielded different Rcrit values depending upon the value of Λ (see Fig. 3). This functional relationship of Rcrit, based on displacement thickness, was plotted versus Λ in Fig. 4 (the plot as far as can be determined from Ref. 1 and Ref. 8 was merely a curve drawn through the indicated stability trials). Schlichting further implied that this relationship for Rcrit vs. Λ, based on various pressure gradients imposed on flat plate flow, could be universally applied to <u>all</u> external boundary layer flows.

The assumption of a universal relationship between Rcrit and Λ as given in Fig. 2 was tested by considering the "wedge flow" cases, which are particular solutions of similar solutions of boundary layer flow. These flows experience a streamwise pressure gradient that is due to a flow area change where the conventional parameter is Hartree's β. Hartree's β is physically interpretted as the ratio of the wedge angle over and is a function of the exponent of the stream-wise coordinate for similar flows denoted in the following form:

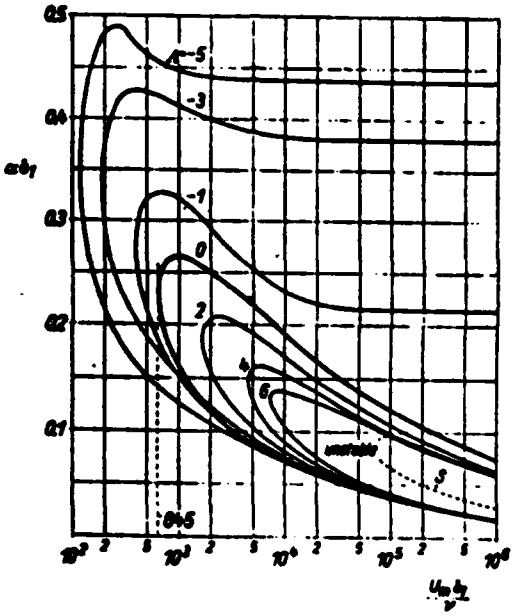

Fig 3 Neutral Stability Curves for Flat Plate with Pressure Gradients. (Ref. 1)

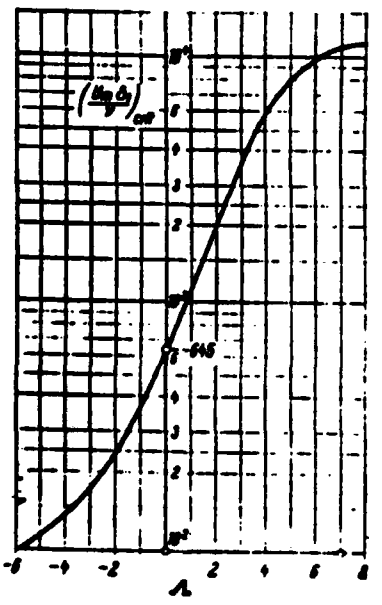

Fig 4 Critical Reynolds Number Variation with Pressure Gradient Factor, Λ. (Ref. 1)

$$\beta = \frac{2m}{m + 1} \tag{8}$$

The relationship between Λ and β (see Appendix B for a full derivation) was found to be

$$\Lambda = \frac{m}{2}(\eta_\delta)^2 \beta(m + 1) \tag{9}$$

where η_δ is the value of the nondimensional coordinate at the edge of the boundary layer (where $u(\eta)$ is 99% of Um). With this relationship it was possible to compare on one plot (see Fig. 5) both the flat plate cases and the wedge flow results and to verify that what Schlichting implied but did not prove appeared to be correct.

The two internal flow cases of two parallel infinite flat plates (plane Poiseuille flow) and fully-developed pipe flow (Hagen-Poiseuille flow) were also considered in this study. There was a stability result available for the parallel flat plate case (Ref. 6) but the pipe flow case was found to be stable to infintesimal disturbances up to all critical Reynolds numbers tried (Ref. 9) and no stability result was thus available. However, a corresponding approximate parameter was estimated for both cases due to the availability of transition data for both cases. This approximate method followed from the known exact solutions of the Navier-Stokes equations (Ref 1:85-86) for Poiseuille flow of

$$u(y) = \frac{-h^2}{2\mu}\left(\frac{dP}{dx}\right)\left(1 - \left(\frac{y}{\eta}\right)^2\right) \tag{10}$$

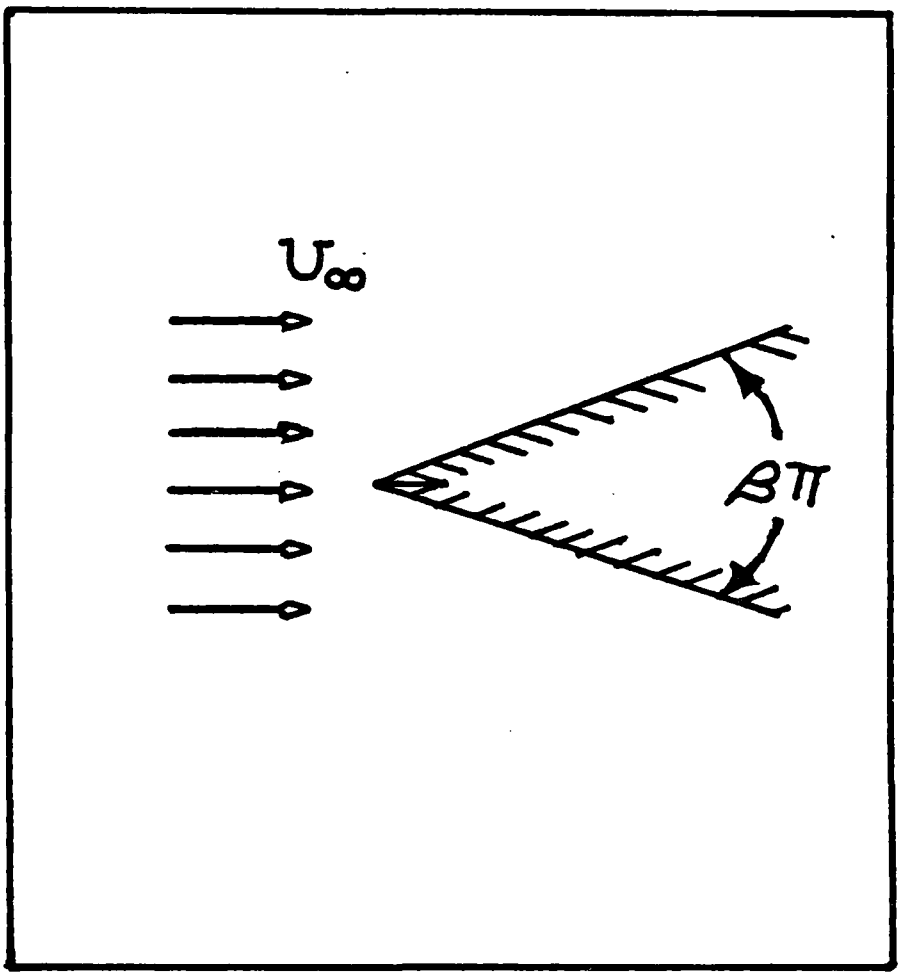

Fig 5 Physical Definition of the Wedge angle.

and for Hagen-Poiseuille flow in a pipe given by

$$u(y) = \frac{-R^2}{4\mu}\left(\frac{dP}{dx}\right)\left(1 - \left(\frac{y}{R}\right)^2\right) \qquad (11)$$

where y is a coordinate measured from the centerline, x is the streamwise coordinate, h is half the distance between the parallel plates, and R is the radius of the pipe. The relationship between the pressure gradient and from equation (5), with the substitution of U centerline for Um and h and R respectively for δ, was adapted wholesale to obtain "equivalent" values of Λ for the parallel plates and the fully-developed pipe flow, which were respectively, $\Lambda = 2$ and $\Lambda = 4$. The values of Λ obtained were those necessary to be consistant with the parabolic velocity distributions commonly given for these flow cases.

Thicknesses

For the external flow cases the different boundary-layer thicknesses were defined in the usual manner. The usual boundary-layer thickness, δ, was the distance out from the wall at which the local velocity had obtained 99% of the "free-stream" velocity value. The displacement thickness, $\delta 1$, was given by

$$\delta 1 = \int_0^\infty \left(1 - \frac{U(\eta)}{U_\infty}\right) d\eta \qquad (12)$$

And, the momentum thickness, $\delta 2$, was given by:

$$\delta 2 = \int_0^\infty \frac{U(\eta)}{U_\infty} \left(1 - \frac{U(\eta)}{U_\infty}\right) d\eta \qquad (13)$$

The flow thicknesses for the interior flow cases were obtained by modifying the conventional definitions given above. The boundary layer thickness, δ, was assumed to be half the flow passage dimension for both the fully-developed internal flow cases. A detailed analysis of the approximations for $\delta 1$ and $\delta 2$ of both internal flow cases is given in Appendix C. The values for the parallel flat plates were approximately $\delta 1 = h/3$ and $\delta 2 = h/7.5$ where h was half the plate separation, and the values for the fully-developed pipe flow were approximately $\delta 1 = (0.293)R$ and $\delta 2 = (0.1835)R$, where R was the pipe radius.

Correlation

The determination of the approximate value of the displacement thickness for the parallel plates case along with its "equivalent" Pohlhausen parameter allowed the inclusion of another stability theory result (Ref. 6) on the plot representing the variation of Rcrit with Λ (see Fig. 5). As can be seen this plot, the internal flow result seem to be consistent with the external flow cases for this work's interpretation of Λ.

Since most transition data appeared to be reported in terms of $R\delta 2$ and not $R\delta 1$, the stability results were

converted into critical Reynolds numbers based on $\delta 2$ (see Fig. 6). An analytic equation was then determined that fit the stability results that was given by

$$R\delta_2,crit = 2954 \tanh \left(\frac{\Lambda - 4.5}{2.7}\right) + 2981 \qquad (14)$$

and was presented with the stability results in Fig. 7.

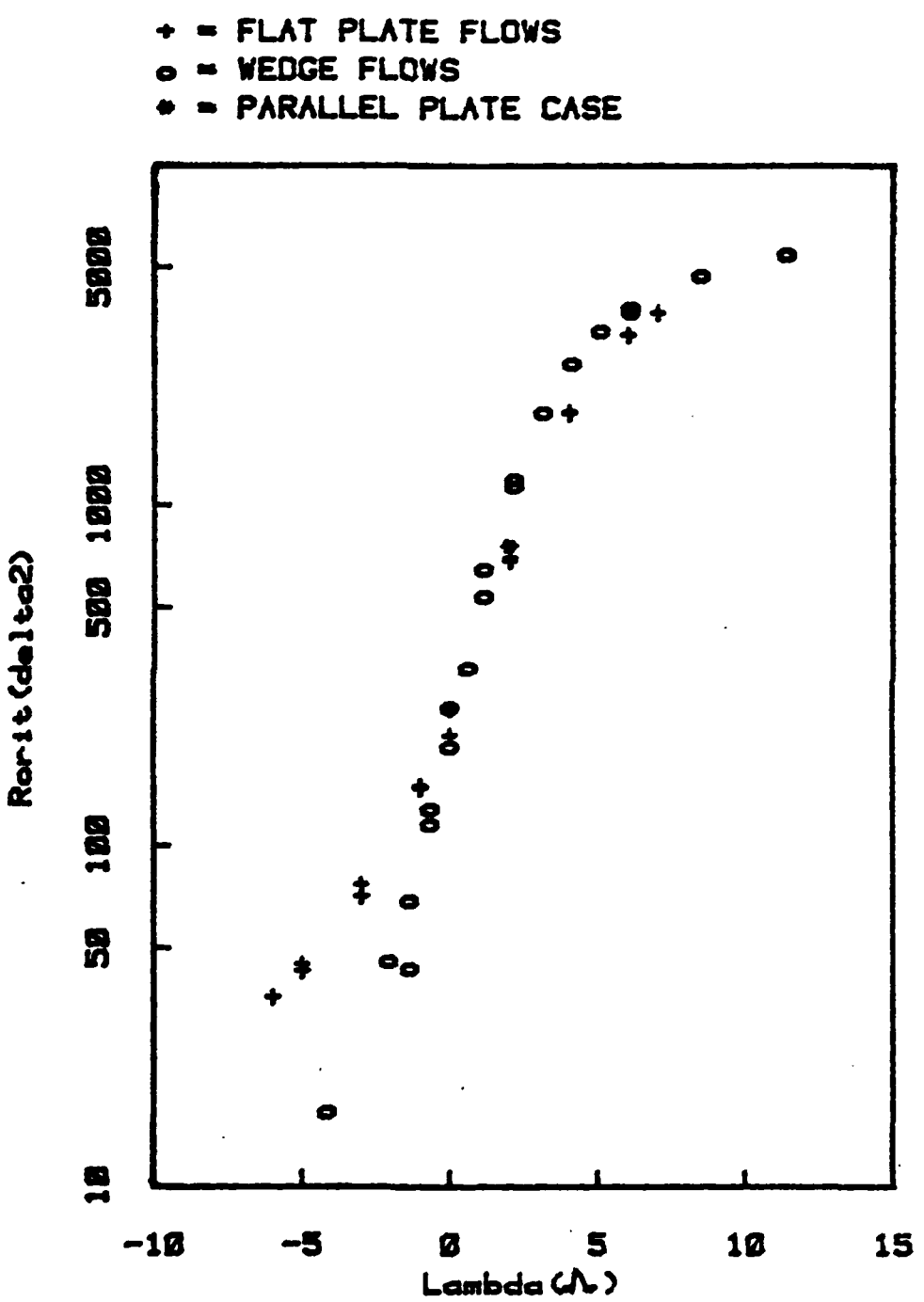

Fig 8 Combined Stability Results.

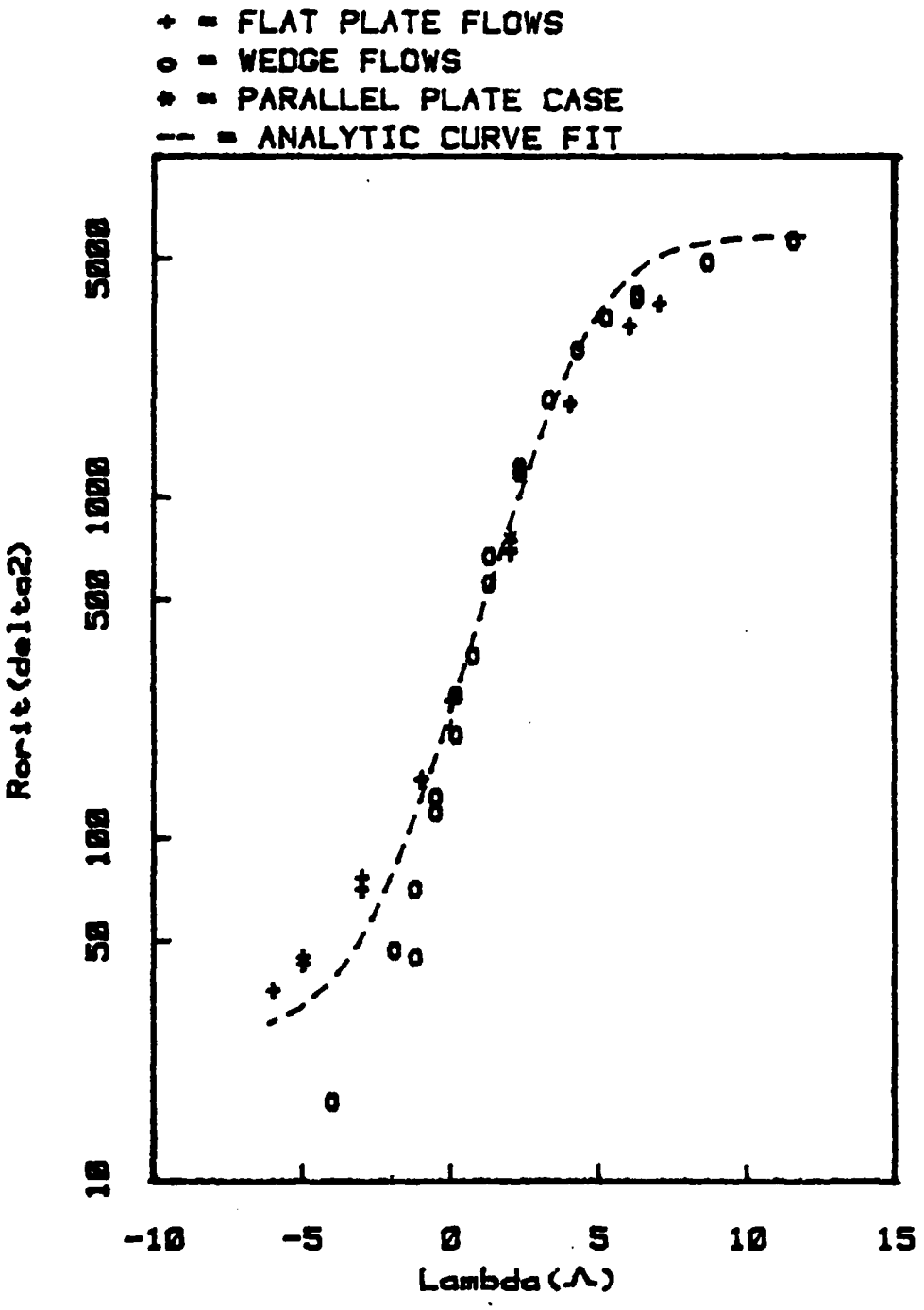

Fig 7 Analytic Stability Curve.

IV. Vorticity Stability

Concurrently with the work done to produce an analytic expression for the wave stability dependence on the ambient pressure gradient, the stability of the vorticity of the flow was also investigated. The laminar flows considered in this work were assumed to be parallel. General turbulent flow, however, is known to be greatly unparallel locally where large vortices feeding "large eddies" break up the main flow and in turn devolve into "small eddies" that are responsible for turbulence on a local level (Ref. 10). As long as the viscous stresses acting against the flow counter-balance the flow's inclination to rotate and form eddies, the main mechanism of turbulent flow motion, eddy production, cannot be sustained and the flow remains laminar. The objective of the work done in this section was to determine a means of predicting when the flow would "trip" over into eddy motion (rotating pockets of fluid) and thus become turbulent.

The anlaysis of the effect of vorticity upon flow transition was based upon a rough visualization of the flow as a solid element moving along a resisting surface (Fig. 8). As long as the moment due to the element's weight counters the inertial moment, the element will tend only to translate along the contact surface. If however the element is elongated away from the contact surface, the weight

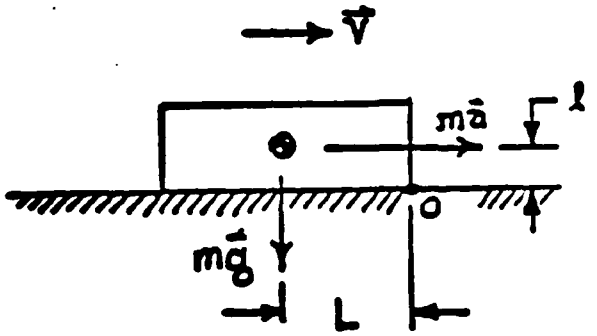

Fig 8a Positive Stability -- Translation: $mgL > mal$

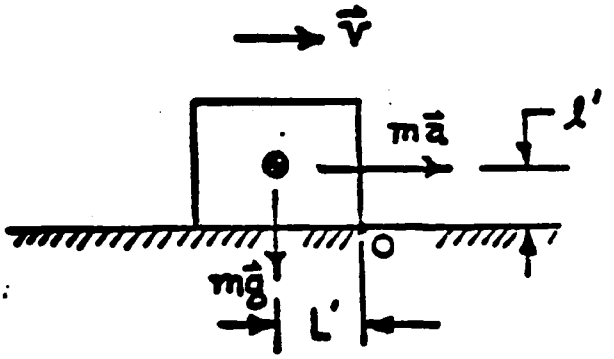

Fig 8b Neutral Stability -- Translation: $mgL' = mal'$

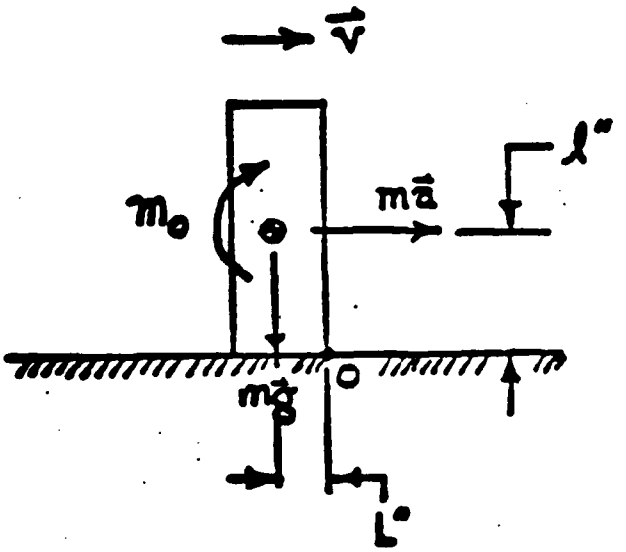

Fig 8c Instability -- Translation and Rotation: $mgL" < mal"$

Fig 8 Physical Analogy of Vorticity Stability

moment will decrease and the inertial moment will increase (Fig. 8b). If this deformation is continued until the inertial moment is greater than the weight moment (Fig. 8c), the element will tend to rotate as well as translate. When this solid element is now considered as an incompressible fluid element, the inertial moment corresponds to the product of the shear stress (proportional to the vorticity) in the fluid and its location away from the flow passage wall. The flow (which is the summation of all of these infinitesimal moving fluid elements) is considered to be unstable when the first moment of the flow vorticity is greater than the effect of the net balancing forces acting on the fluid element (Ref. 11). While these balancing forces are not identified specifically, it is hypothesized that they are dependent on fluid properties but independent of local flow conditions; that is to say, once the first moment of vorticity gets to be some magnitude, the flow becomes unstable.

The vorticity of the parallel flows considered was given by

$$\zeta = \nabla \times \vec{v} = \left(\frac{\partial v}{\partial x} - \frac{\partial u}{\partial y}\right) \tag{14}$$

which, if $\partial v/\partial x$ is neglected, was simplified to

$$\zeta = - \frac{\partial u}{\partial y} \tag{15}$$

The first moment of vorticity was designated as I, where I was defined by

$$I = \frac{1}{\nu} \int_0^{\delta} - \zeta y dy \qquad (16)$$

The viability of this approach was tested by considering the Pohlhausen boundary-layer profile and the parabolic velocity profile for fully-developed parallel plate flow. In the first case, the velocity profile was given by

$$u(y) = U \left(\frac{2y}{\delta} - \frac{2y^3}{\delta^3} + \frac{y^4}{\delta^4} + \frac{\Lambda}{6}\left(\frac{y}{\delta} - \frac{3y^2}{\delta^2} + \frac{3y^3}{\delta^3} - \frac{y^4}{\delta^4}\right)\right) \qquad (17)$$

The moment, I, was then given by

$$I = \frac{U}{\nu} \int_0^{\delta} \left(\frac{2y}{\delta} - \frac{6y^3}{\delta^3} + \frac{4y^4}{\delta^4} + \right.$$

$$\left. \frac{\Lambda}{6}\left(\frac{y}{\delta} - \frac{6y^2}{\delta^2} + \frac{9y^3}{\delta^3} - \frac{4y^4}{\delta^4}\right)\right) dy \qquad (18)$$

with the result that

$$I = \frac{U\delta}{\nu}\left(\frac{3}{10} - \frac{\Lambda}{120}\right) \qquad (19)$$

Using the shape-factor ratio of δ_1 to δ given by Pohlhausen (Ref. 1) as (3/10 - Λ/120), this measure of stability was then $I = R_{\delta_1}$, or the Reynolds number basedon the displacement thickness. The second case used a velocity profile given by

$$u(y) = U\left(\frac{2y}{h} - \frac{y^2}{h^2}\right) \tag{20}$$

where half the displacement between the plates, h, was equated to the boundary-layer thickness, δ. The moment, I, was then given by

$$I = \frac{U}{\nu} \int_0^{\delta} \left(\frac{2y}{\delta} - \frac{2y^2}{\delta^2}\right) dy \tag{21}$$

and resulted in,

$$I = \frac{1}{3} \frac{U\delta}{\nu} \tag{22}$$

When compared with the shape-factor previously determined for the parallel plates case of 1/3, I again was the value of the Reynolds number based on the boundary-layer displacement thickness, $R_{\delta 1}$. These results indicated that the value of the Reynolds number based on displacement thickness was the single parameter for flow stability.

V. Results

The validity of the two prediction methods was examined by comparing the predicted results with those available from experimental investigations in two different ways. The prediction results were first compared to accumulated data for a variety of different airfoils and flow cases and then the prediction methods were used to analytically estimate the location of the transition point for a NACA 0018 airfoil that experienced two different body Reynolds numbers and different angles of attack.

Pressure Gradient Method

The pressure gradient method that was derived from stability theory was converted into transition data in two different ways. Initially the analytic curve that fit the stability data,

$$R_{\delta 2,crit} = 2954 \tanh \left(\frac{\Lambda - 4.5}{2.7}\right) + 2981 \qquad (23)$$

was converted to a transition basis by scaling the predicted critical value of $R_{\delta 2,crit} = 231$ for the zero pressure gradient case ($\Lambda = 0$) to the transition value of $R_{\delta 2,trans} = 1150$. This transition value was obtained by modifying the Kays and Crawford method (Ref. 1) where a value for Rx,trans = 3,000,000 was used instead of their value, Rx,trans = 300,000 (this higher value is

experimentally supported by Reference 12). The resulting analytic equation was then:

$$R_{\delta 2,trans} = 14786 \tanh\left(\frac{\Lambda - 4.5}{2.7}\right) + 14917 \qquad (24)$$

The second method took into account the known difference between $R_{\delta 2,crit}$ and $R_{\delta 2,trans}$ shown in Figure 9 (Ref. 13). An analytic curve fit for this difference was found to be

$$\Delta R_{\delta 2} = 400 \exp(60\lambda) + 400 \qquad (25)$$

where λ was related to Λ (Ref 2:210) by

$$\lambda = \left(\frac{37}{315} - \frac{1}{945}\Lambda - \frac{1}{9072}\Lambda^2\right)^2 \Lambda \qquad (26)$$

This difference was then added to the $R_{\delta 2,crit}$ expression of equation (23) to obtain a transition Reynolds number of the form:

$$R_{\delta 2,trans} = 2954 \tanh\left(\frac{\Lambda - 4.5}{2.7}\right) + 2981 + \Delta R_{\delta 2} \qquad (27)$$

The results of both of these methods are shown in Figure 10, together with experimental results which were taken from Reference 14. (It must be noted that the expression for $\Delta R_{\delta 2}$ was only valid for λ values less than 0.025, or Λ values less than 2.0, and subsequently care should be taken when using that method of conversion.)

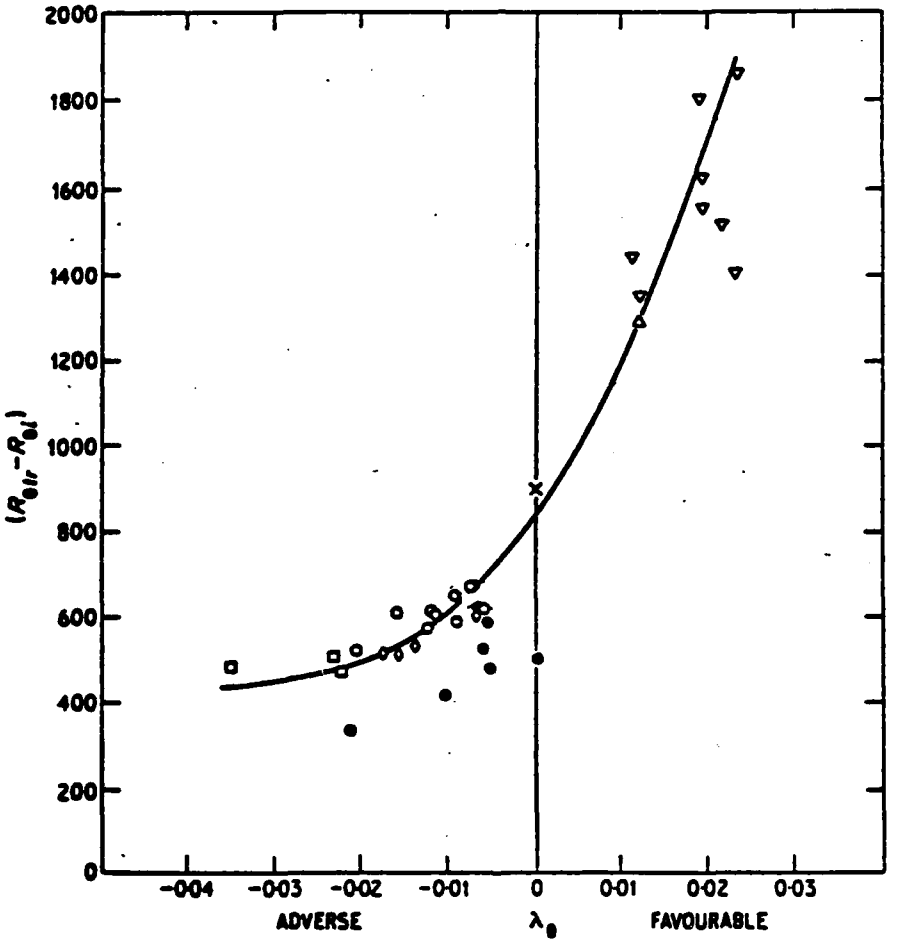

Fig 9 Empirical ΔR Variation with λ. (Ref. 13)

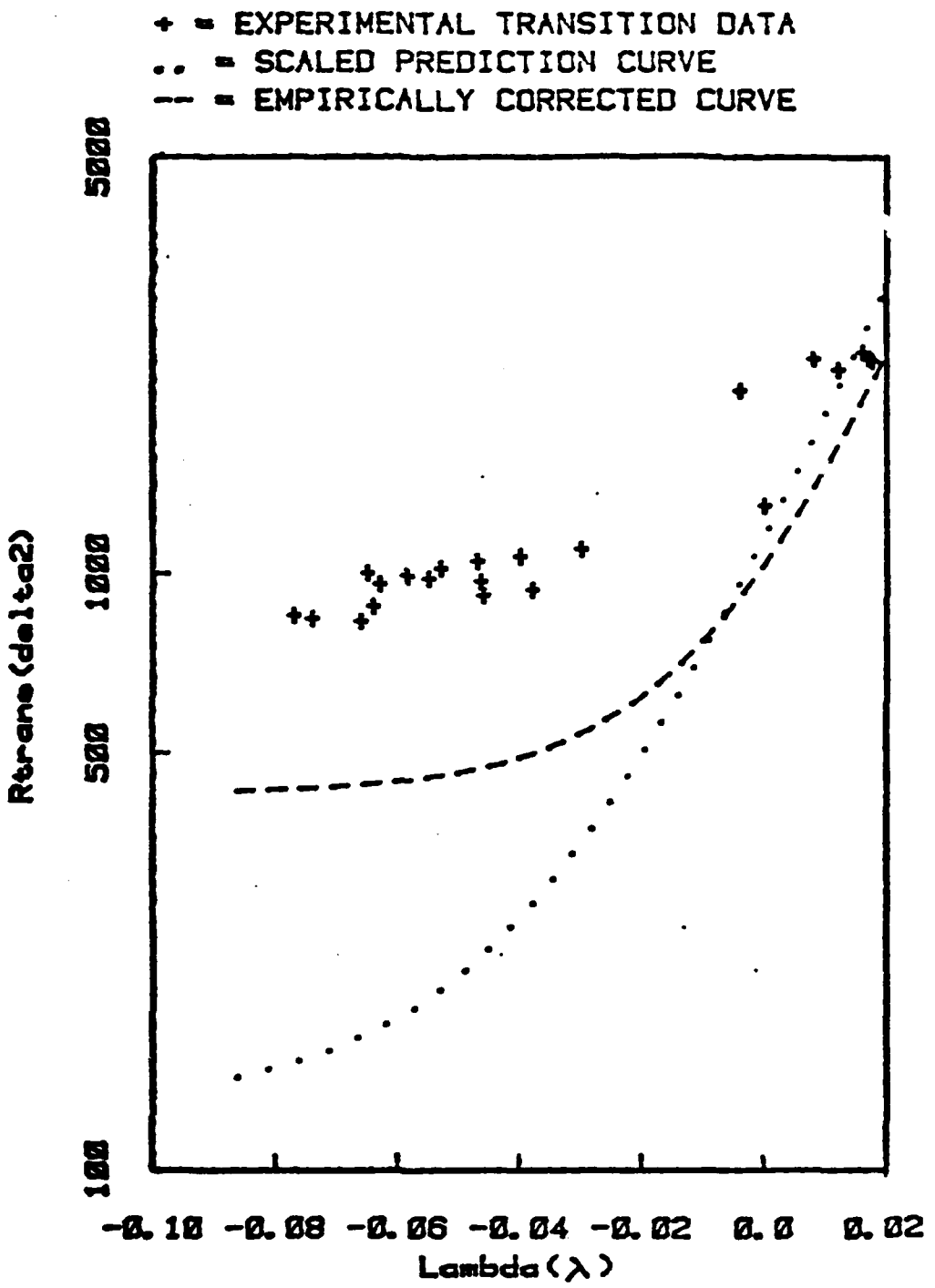

Fig 10 Comparison of Stability-Derived Curves with Data.

Vorticity Stability Method

Two values of $R_{\delta 1,trans}$ = constant were chosen to represent the vorticity-stability theory; a value or $R_{\delta 1}$ = 3000 that corresponded to low (0%) free-stream turbulence levels and a value of R_{1} = 1226 that corresponded to high (1.2%) free-stream turbulence levels. These values were chosen so as to be consistent with the findings of Hall and Gibbings (Ref. 13). A shape-factor consistent with Pohlhausen's polynomial fit (Ref. 1:210) was used to relate $R_{\delta 2}$ to $R_{\delta 1}$ by the function

$$R_{\delta 2} = R_{\delta 1} \frac{\frac{37}{315} - \frac{1}{945}\Lambda - \frac{1}{9075}\Lambda^2}{\frac{3}{10} - \frac{1}{120}\Lambda} \qquad (28)$$

The resulting variations of $R_{\delta 2,trans}$ with λ are shown in Figure 11 along with previous results and further data (from Ref. 13). It was evident that a constant value of $R_{\delta 1}$ fit the data for $\lambda < 0$ (adverse pressure gradients) quite well but tended to underestimate the value for $R_{\delta 2,trans}$ for $\lambda > 0$ (favorable pressure gradients). This lack of correlation for vorticity stability to experimental data for accelerated flow might be due to the limitations of a fourth order polynomial fit for the velocity profile in this region or might be due to other undetermined reasons. It is interesting to note, however, that in the favorable pressure gradient region the transition equations based on

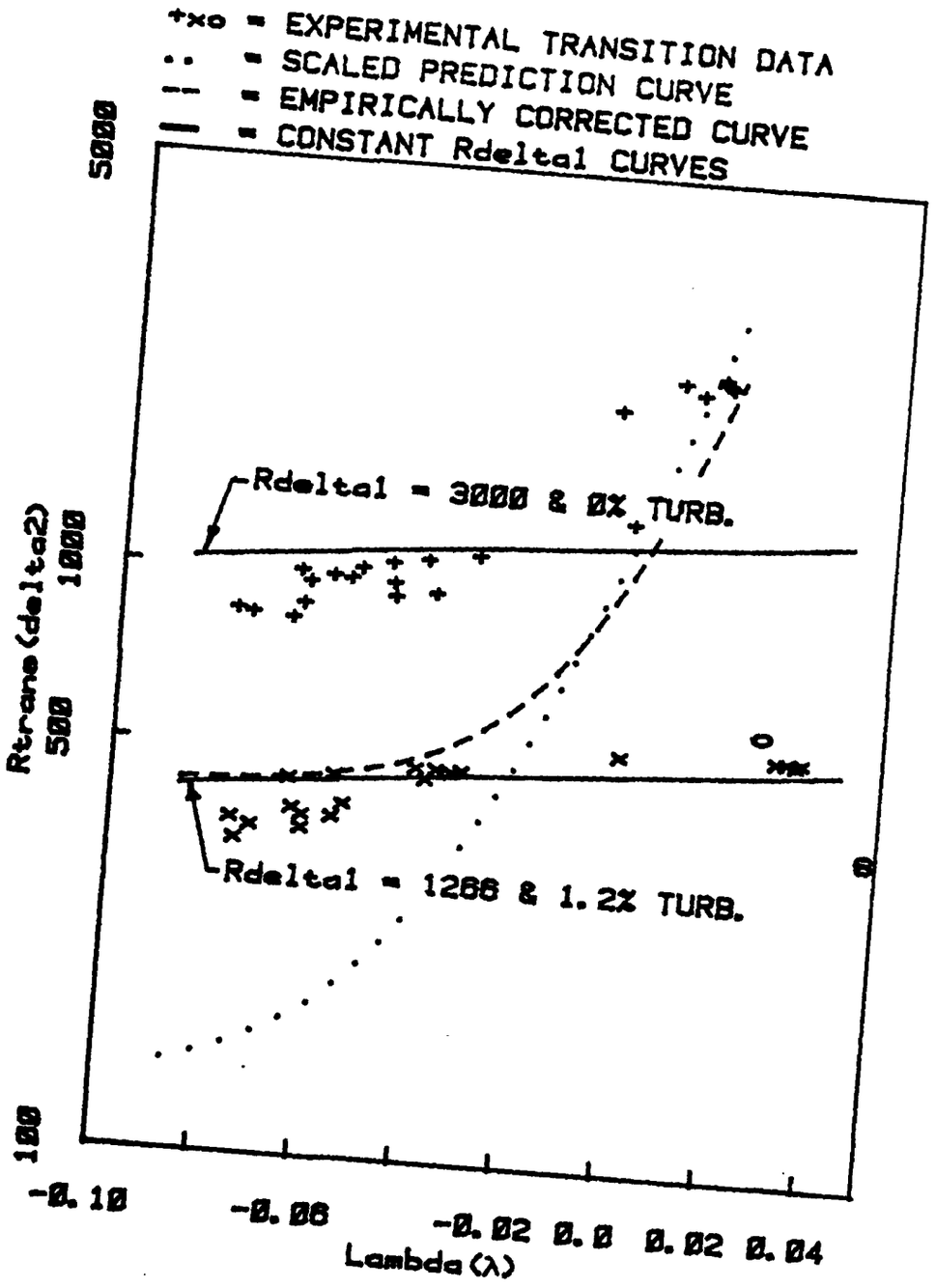

Fig 11 Prediction Curves and Data.

wave-stability fit the low-level free-stream turbulence data. It is possible that wave mechanics effects overshadow the effects of vorticity-stability of the flow for these cases.

The two values of $R_{\delta 1}$ = constant, 3000 and 1226, that are presented in Fig. 11 are arbitrary bracketing cases for the data. These values in turn represent flat plate Reynolds numbers based on the location from the leading edge of 363,000 and 3,130,000 respectively, which are within reported experimental limits of experimental flat plate, zero pressure gradient, transition (Ref. 12).

Internal Flow Results

The two internal flow results considered in this work concerned parallel flow between two infinite plates and fully-developed flow in a pipe. The parallel plates result was based on a thin rectangular duct study where the aspect ratio was 8:1 (width/depth) and the transition Reynolds number based on average velocity and hydraulic diameter was experimentally found to be 2600 (Ref. 15). This Reynolds number yielded $R_{\delta 2,trans}$ = 585. The pipe flow result was based on the universally quoted value of the Reynolds number, based on hydraulic diameter and average velocity, of 2000 for transition. This value yielded a value of $R_{\delta 2,trans}$ = 366. both of these results are shown in Fig. 11 and signified by "o". It is interesting to note that the low-level free-stream turbulence value of $R_{\delta 1}$ = constant

(3000) yielded a $R_{d,trans} = 6853$, which is well within the known experimental range of 2000 to 40,000 (Ref. 16).

Prediction of Transition Location

The prediction methods developed in this work were used to estimate the location of transition on a NACA 0018 airfoil. Schlichting (Ref. 1:500) gave a presentation where the experimental transition curves of two body Reynolds numbers, those of 1,700,000 and 5,000,000, for the NACA airfoil were compared with stability curves of a Joukowski 0015 airfoil that had a similar pressure distribution. The work presented here used a computer program (which was obtained from Captain J. Lawrence, Ref. 17) that calculated boundary-layer parameters at incremental steps along a Joukowski airfoil. At various angles of attack, estimates were then made to locate the transition points on the airfoil for the various angles of attack and resultant coefficients of lift. Transition curves for both a $R_{\delta 1}$ value of 1355 and the scaled pressure gradient dependent method, Equation (24), were used to produce the results presented in Figures 12 and 13. It can be seen in both cases that the predicted transition curves did a better job at predicting transition than the stability curves alone. The constant $R_{\delta 1}$ curve gave a closer approximation to the experimental curve for the $R_1 = 1.7$ million case but did not do as well as the pressure gradient dependent method for the $R_1 = 5.0$ million case.

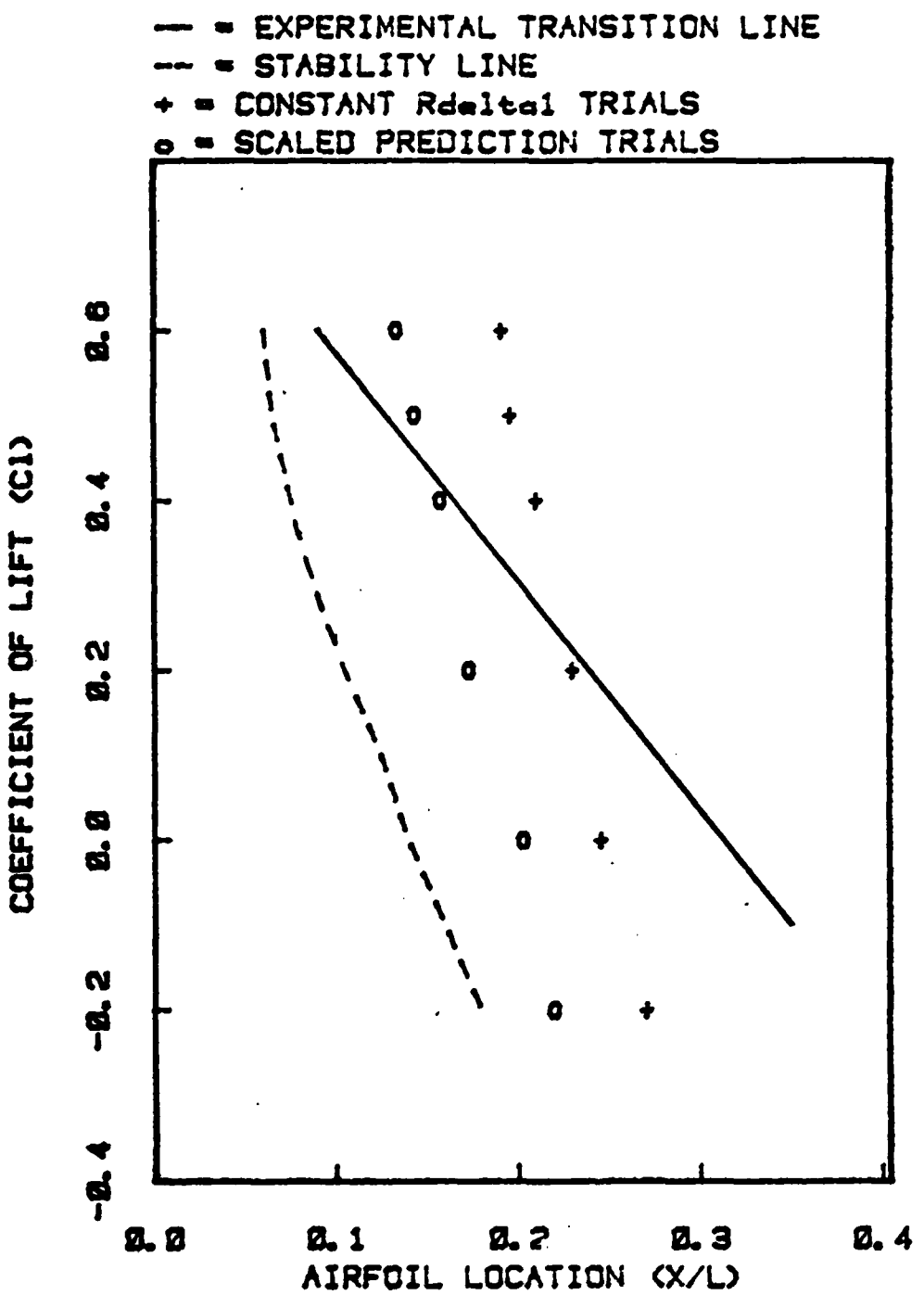

Fig 12 Prediction Trials for R1=1.7mil.

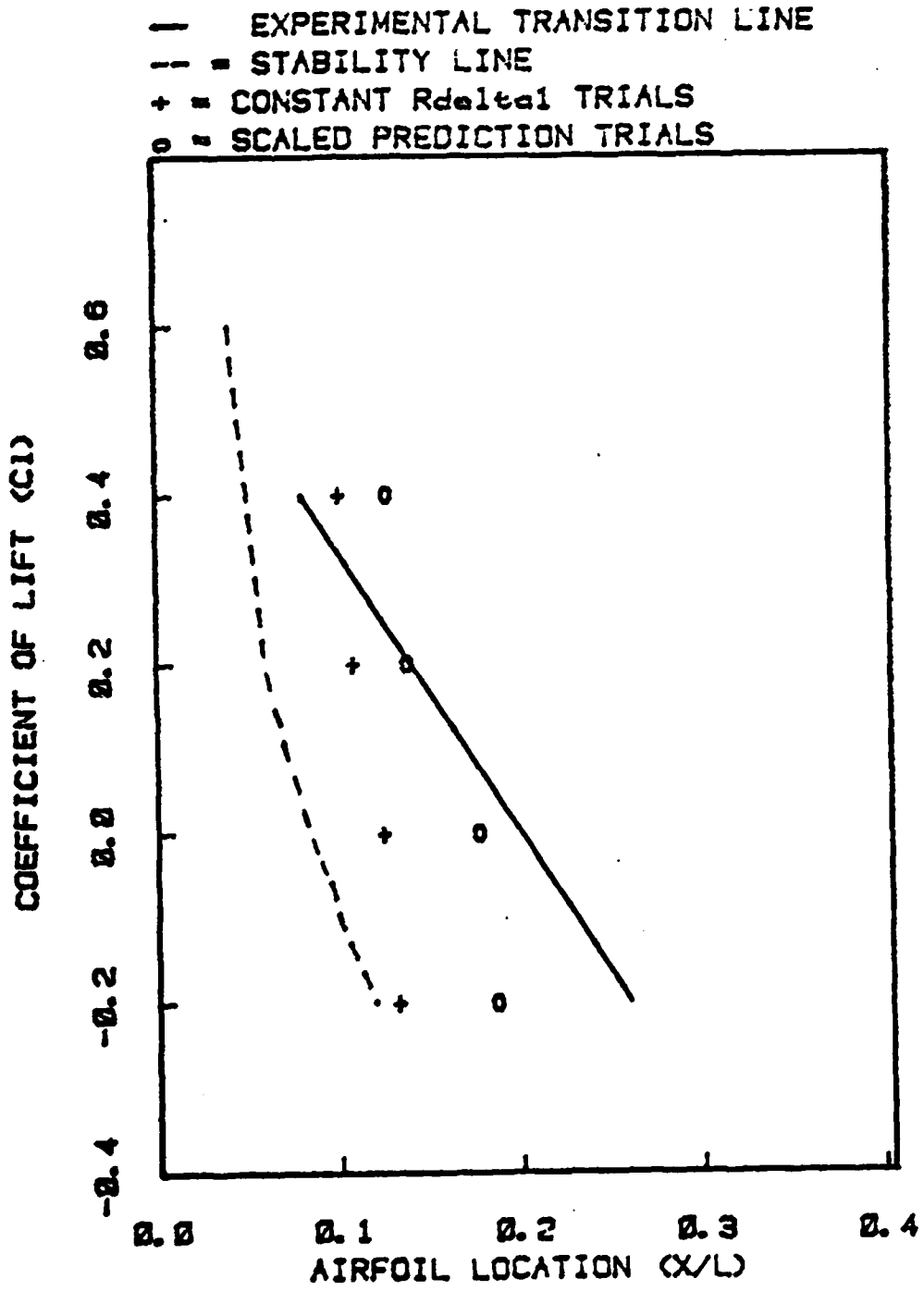

Fig 13 Prediction Trials for R1=5.0mil.

VI. Conclusions and Recommendations

This work produced two different methods for predicting the transition of laminar to turbulent flow. The first approach resulted in a pressure gradient dependent technique that matched the available experimental data well in the region of adverse pressure gradients but underestimated the data for favorable pressure gradients. The second method, derived from viewing the stability of the flow's vorticity, resulted in a criterion of a constant Reynolds number, based on boundary-layer displacement thickness, that fit the data well for favorable pressure gradients but underestimated the data for adverse pressure gradient cases.

Future work in this area could include a more rigorous examination of the modelling techniques, a high-order polynomial fit for the velocity profile, e.g., that might improve the prediction results for both methods. In addition Hall and Gibbings (Ref. 13) noted that $R_{\delta 1,trans}$ varied with free-stream turbulence levels. This variation could be investigated further or the effect of other parameters, such as heat transfer, upon $R_{\delta 1}$ could be examined.

Appendix A

Orr-Sommerfeld Equation Derivation

The Orr-Sommerfeld equation is based on the three-dimensional, nonsteady, encompressible Navier-Stokes equations, as follows:

$$\rho\left(\frac{\partial u}{\partial t} + u\frac{\partial u}{\partial x} + v\frac{\partial u}{\partial y} + w\frac{\partial u}{\partial z}\right) = X - \frac{\partial P}{\partial x} + \mu\nabla^2 u \qquad \text{(A1)}$$

$$\rho\left(\frac{\partial v}{\partial t} + u\frac{\partial v}{\partial x} + v\frac{\partial v}{\partial y} + w\frac{\partial v}{\partial z}\right) = Y - \frac{\partial P}{\partial y} + \mu\nabla^2 v \qquad \text{(A2)}$$

$$\rho\left(\frac{\partial w}{\partial t} + u\frac{\partial w}{\partial x} + v\frac{\partial w}{\partial y} + w\frac{\partial w}{\partial z}\right) = Z - \frac{\partial P}{\partial y} + \mu\nabla^2 v \qquad \text{(A3)}$$

$$\frac{\partial u}{\partial x} + \frac{\partial v}{\partial y} + \frac{\partial w}{\partial z} = 0 \qquad \text{(A4)}$$

Simpliflying assumptions are that body forces are negligible and that there is only one-dimensional mean flow in the x-direction. The total flow variables are sums of mean and perturbation quantities of the form:

$$u = \bar{u}(y) + u'$$

$$v = v'$$

$$w = w'$$

$$P = P + P'$$

These variables are substituted back into the Navier-Stokes equations with only the terms linear in u', v', or w' retained. The equations are now of the form:

$$u'_t + \bar{u}u'_x + v'\bar{u}_y = -\frac{P'_x}{\rho} + \nu\nabla^2 u' \tag{A5}$$

$$v'_t + \bar{u}v'_x = -\frac{P'_y}{\rho} + \nu\nabla^2 v' \tag{A6}$$

$$w'_t + \bar{u}w'_x = -\frac{P'_z}{\rho} + \nu\nabla^2 w' \tag{A7}$$

$$u'_x + v'_y + w'_z = 0 \tag{A8}$$

The disturbances are considered to be bounded as x and z tend toward infinity. They are also considered spatially periodic of the form

$$u' = \tilde{u}(y,t)\exp[i(kx + lz)]$$
$$v' = \tilde{v}(y,t)\exp[i(kx + lz)]$$
$$w' = \tilde{w}(y,t)\exp[i(kx + lz)]$$
$$P' = \tilde{P}(y,t)\exp[i(kx + lz)]$$

The equations are now

$$\tilde{u}_t + \bar{u}(ik\tilde{u}) + \tilde{v}Uy = -ik\frac{\tilde{P}}{\rho} + \nu(-k^2 - l^2 + \tilde{u}_{yy}) \tag{A9}$$

$$\tilde{u}_t + \bar{u}(ik\tilde{v}) = -\frac{\tilde{P}_y}{} + \nu(-k^2 - l^2 - \tilde{v}_{yy}) \tag{A10}$$

$$\tilde{w}_t + \bar{u}(ik\tilde{w}) = -\frac{il\tilde{P}_z}{\rho} + \nu(-k^2 - l^2 - \tilde{w}_{yy}) \tag{A11}$$

$$ik\tilde{u} + \tilde{v}_y + il\tilde{w} = 0 \tag{A12}$$

Equation A9 is multiplied by $k/(k^2 + l^2)^{1/2}$ and equation A11 is multiplied by $l/(k^2 + l^2)^{1/2}$ and the two are added together to yield:

$$\frac{\partial}{\partial t}(k\tilde{u} + l\tilde{w}) + \bar{u}(ik)(k\tilde{u} + l\tilde{w}) - \bar{u}_y k\tilde{u} =$$

$$i(k^2 + l^2)\frac{\tilde{P}}{\rho} + \nu[-k^2(k\tilde{u} + l\tilde{w}) - l^2(k\tilde{u} + l\tilde{w})$$

$$+ \frac{\partial^2}{\partial y^2}(k\bar{u} + l\tilde{w})] \qquad \text{(A13)}$$

New variables are now defined as

$$\hat{u} = \frac{k\tilde{u} + l\tilde{w}}{(k^2 + l^2)^{1/2}}, \quad \alpha^2 = k^2 + l^2, \quad \hat{P} = \frac{\alpha\tilde{P}}{k}, \quad \hat{t} = \frac{kt}{\alpha}$$

where the equations are now of the form:

$$\hat{u}_t + \bar{u}(i\alpha\hat{u}) + \hat{v}\bar{u}_y = -i\alpha\frac{\hat{P}}{\rho} + \frac{\nu\alpha}{k}(-\alpha^2 + \hat{u}_{yy}) \qquad \text{(A14)}$$

$$\tilde{v}_t + \bar{u}(i\alpha\tilde{v}) = -\alpha\frac{\hat{P}y}{\rho} + \frac{\nu\alpha}{k}(-\alpha^2 + \tilde{v}_{yy}) \qquad \text{(A15)}$$

$$i\alpha\hat{u}_x + \tilde{v}_y = 0 \qquad \text{(A16)}$$

Equations A14-A16 are now of the form of equations A9-A12 if $\tilde{w}$ and l are zero, which is the form of the two-dimensional perturbation case. Since $(\alpha/k)\nu = ((k^2 + l^2)/k)\nu > \nu$, then $R_{crit\text{-}2d} < R_{crit\text{-}3d}$ and two-dimensional perturbations are less stable than three-dimensional ones. This result is known as Squire's theorem. Further analysis can be simplified conservatively, therefore, by considering only two-dimensional perturbations.

If equations A9, A10, and A12 are taken with $\tilde{w} = 0$ and the mean flow equations are assumed to satisfy the N.S. equations, i.e.,

$$\frac{1}{\rho}\frac{\partial P}{\partial x} = \nu \frac{d^2\bar{u}}{dy^2} \quad \text{and} \quad \frac{1}{\rho}\frac{\partial P}{\partial y} = 0$$

then the N.S. equations are then of the form:

$$u'_t + \bar{u}u'_x + v'\bar{u}_y + 1/\rho\, P'_x = \nu\nabla^2 u' \qquad \text{(A17)}$$

$$v'_t + \bar{u}v'_x + 1/\rho\, P'_y = \nu\nabla^2 v' \qquad \text{(A18)}$$

$$u'_x + v'_y = 0 \qquad \text{(A19)}$$

A stream function, ψ, is now introduced

$$\psi(x,y,t) = \phi(y)\exp[i(\alpha x - \beta t)]$$

where

ϕ = complex amplitude

$\alpha = \frac{2\pi}{\lambda}$ (wave number)

$\beta = \beta_r + i\beta_i$

β_r = circular frequency of partial oscillation

β_i = amplification factor

$C = \beta/\alpha$

C_r = velocity of wave propagation in x-direction

C_i = degree of amplification/damping

The perterbation velocities are now defined by

$$u' = \frac{\partial \psi}{\partial y}$$

$$= \phi'(y)\exp[i(\alpha x - \beta t)]$$

$$v' = -\frac{\partial \psi}{\partial x}$$

$$= -i\alpha\phi(y)\exp[i(\alpha x - \beta t)]$$

substituting back into A17, A18, and A19 yields

$$\phi(-i\beta)\exp[i(\alpha x - \beta t)] + \bar{u}\phi' i\alpha\exp[i(\alpha x - \beta t)]$$

$$- i\alpha\phi\exp[i(\alpha x - \beta t)]u' + \frac{P_x}{\rho}$$

$$= \nu(-\phi'\alpha^2\exp[i(\alpha x - \beta t)] + \phi'''\exp[i(\alpha x - \beta t)]) \quad \text{(A20)}$$

$$-\alpha\beta\phi\exp[i(\alpha x - \beta t)] + \bar{u}\alpha^2\phi\exp[i(\alpha x - \beta t)] + \frac{P_y}{\rho}$$

$$= \nu(iU\alpha^3\phi\exp[i(\alpha x - \beta t)] - i\alpha\phi'''\exp[i\alpha x - \beta t)] \quad \text{(A21)}$$

$$\phi'(i\alpha)\exp[i(\alpha x - \beta t)] - (i\alpha\phi'\exp[i(\alpha x - \beta t)] = 0 \quad \text{(A22)}$$

If equation A20 is differentiated with respect to y, Equation A21 is differentiated with respect to x, the pressure term is assumed to be indifferent to order of differentiation, the resultant Equation A21 is subtracted from the new Equation A20, and the resultant combined equation is divided through by exp(i(αx - βt)), then the single combined equation is of the form:

$$i\beta\phi'' + i\alpha\bar{u}\phi'' - i\alpha\phi\bar{u}'' + i\alpha^2\beta\phi - i\alpha^3\bar{u}\phi =$$

$$\nu(\phi'''' - 2\phi''\alpha^2 + \alpha^4\phi) \quad \text{(A23)}$$

And finally, if Equation A23 is divided through by $i\alpha$ (where

$C = \beta/\alpha$), nondimensionalized by $R = 1Um/\nu$, and the terms on the left-side of the equation rearranged, the common form of the Orr-Sommerfeld equation is produced as:

$$(\bar{u} - c)(\phi'' - \alpha^2\phi) - \bar{u}''\phi$$

$$= -\frac{i}{\alpha R}(\phi'''' - 2\alpha^2\phi + \alpha^4\phi) \qquad \text{(A24)}$$

Appendix B

Conversion of β Parameter To Λ Parameter

Pohlhausen's shapefactor is usually defined as:

$$\Lambda = \frac{\delta^2}{\nu} \frac{dU_m}{dx} \tag{B1}$$

where

δ = boundary-layer thickness

ν = fluid kinematic viscosity

$U_m = U_o x^m$ (U_o = constant)

x = streamwise coordinate

Hartree's beta parameter or wedge angle (see Fig. 5) is defined as (Ref. 1):

$$\beta = \frac{L}{U_\infty} \cdot g^2 \cdot \frac{dU_m}{dx} \tag{B2}$$

where

L = characteristic length

U_∞ = free-stream velocity

and

$$g = \left(\frac{2}{m+1}\right) \left(\frac{x}{L}\right) \left(\frac{U_\infty}{U_m}\right) \tag{B3}$$

If Equation (B3) is substituted into Equation (B2), the resultant expression for Hartree's parameter is

$$\beta = \left(\frac{2}{m+1}\right) \cdot \left(\frac{x}{U_m}\right) \cdot \frac{dU_m}{dx} \tag{B4}$$

Equations (B1) and (B4) are then solved for dU_m/dx to yield:

$$\frac{dU_m}{dx} = \frac{\beta \cdot U_m \cdot (m + 1)}{2 \quad x} = \frac{\Lambda \nu}{\delta^2} \tag{B5}$$

Rearranging yields,

$$\Lambda = \left(\frac{U_m \delta^2}{2 \cdot \nu x}\right) \cdot \beta \cdot (m + 1) \tag{B6}$$

For a given boundary-layer flow, the boundary-layer thickness is given in terms of the similarity variable, η, in the form:

$$\delta = \eta_\delta \sqrt{\frac{\nu x}{U_\infty}} \tag{B7}$$

where η_δ is the value of the similarity variable at the edge of the boundary layer. If U_m is approximated by U_∞ and Equation (B7) is substituted into Equation (B6), the final expression relating Λ to β is given by

$$\Lambda = \frac{(\eta_\delta)^2}{2} \cdot \beta \cdot (m + 1) \tag{B8}$$

Various authors have tabulated values of η_δ variation with β. In this work η_δ values from Reference 18 were used to convert $R_{\delta 1, crit}$ results from References 19 and 7 from a β dependence to a dependence on Λ. These results are given in Table B.

Table B

β	m	n_δ	Λ	$R_{\delta_1,crit}$
1.00	1.000	3.372	11.370	12400
1.00	1.000	3.372	11.370	12490
0.80	0.667	3.564	8.468	10920
0.60	0.429	3.769	6.088	8640
0.60	0.429	3.769	6.088	8890
0.50	0.332	3.899	5.067	7680
0.40	0.250	4.045	4.091	6230
0.30	0.176	4.206	3.122	4550
0.20	0.111	4.393	2.144	2955
0.20	0.111	4.393	2.144	2830
0.10	0.053	4.626	1.126	1658
0.10	0.053	4.626	1.126	1380
0.05	0.026	4.767	0.583	865
0.00	0.000	4.924	0.000	680
0.00	0.000	4.924	0.000	520
-0.05	-0.024	5.244	-0.671	354
-0.05	-0.024	5.244	-0.671	318
-0.10	-0.048	5.356	-1.366	126
-0.10	-0.048	5.356	-1.366	199
-0.14	-0.065	5.624	-2.069	138
-0.199	-0.090	6.771	-4.162	0
-0.199	-0.090	6.771	-4.162	67

Appendix C

Boundary-Layer Thicknesses

For the two internal flow cases the boundary-layer displacement thicknesses and the boundary-layer moment thicknesses were approximated following a method given by Dr. J. Hitchcock (Ref. 20).

A. Parallel Flat Plates

1. Displacement Thickness

The common definition for the boundary-layer displacement thickness was given by:

$$\delta 1 = \int_0^\infty \left(1 - \frac{u(y)}{U}\right) dy \qquad (C1)$$

Here, a flow area was equated to the integration of $(1 - u(y)/U)$ over a differential perimeter area in the form:

$$(\text{flow area}) = \int_{\text{flow area}} \left(1 - \frac{u(y)}{U}\right) d(\text{perimeter area}) \qquad (C2)$$

where from Figure C1a

$$(\text{flow area}) = 2 \cdot w \cdot \delta 1 \qquad (C3)$$

$$d\,(\text{perimeter area}) = 2wdy + 2hdz \qquad (C4)$$

For two infinite parallel plates (Fig. C1b) the differential perimeter area became 2wdy. Using a parabolic distribution for the velocity,

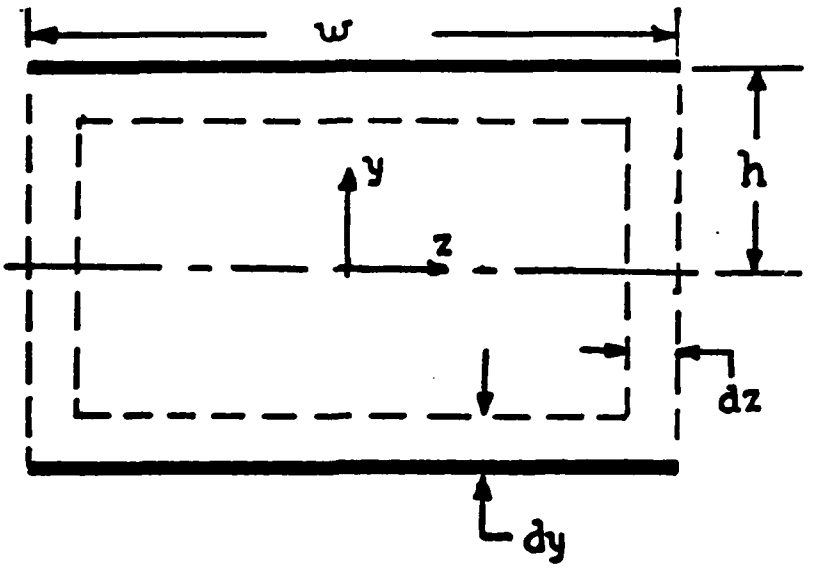

Fig C1a Parallel Plate Dimensions.

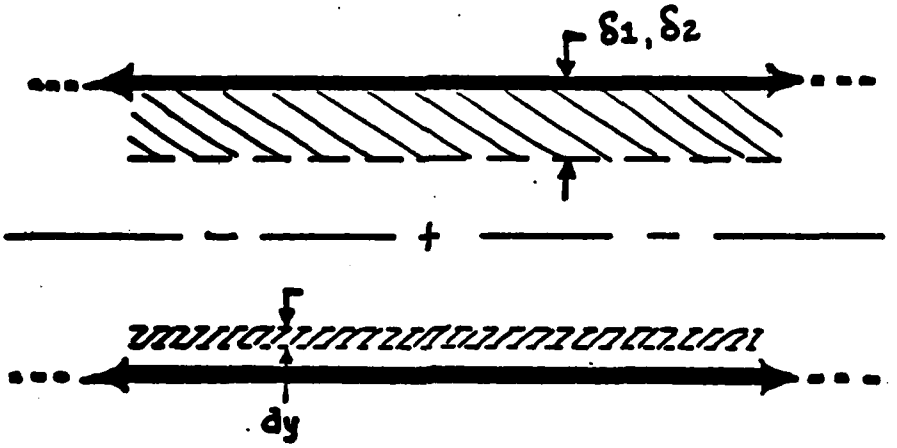

Fig C1b Infinite Parallel Plates.

Fig C1 Parallel Plate Geometry.

$$\frac{u(y)}{U} = \left(\frac{2y}{h}\right) - \left(\frac{y}{h}\right)^2 \qquad (C5)$$

The expression for the displacement thickness was then

$$\delta_1 = \int_0^h \left(1 - \frac{2y}{h} + \frac{y^2}{h}\right) dy \qquad (C6)$$

or,

$$\delta_1 = h/3 \qquad (C7)$$

2. Momentum Thickness

The momentum thickness is commonly given as:

$$\delta 2 = \int_0^\infty \frac{u(y)}{U}\left(1 - \frac{u(y)}{U}\right) dy$$

The approximation used here was

$$\text{(flow area)} = \int_{\text{flow area}} \left(\frac{u(y)}{U}\left(1 - \frac{u(y)}{U}\right)\right) d\,(\text{perimeter area}) \qquad (C8)$$

or,

$$2w\delta 2 = \int_0^h \frac{u(y)}{U}\left(1 - \frac{u(y)}{U}\right)(2w\,dy) \qquad (C9)$$

Again, using a parabolic velocity distribution yielded:

$$\delta 2 = \int_0^h \left(\frac{2y}{h} - \frac{y^2}{h^2}\right)\left(1 - \frac{2y}{h} + \frac{y^2}{h^2}\right) dy \qquad (C10)$$

or,

$$\delta 2 = h/7.5 \qquad \text{(C11)}$$

B. Pipe Flow

1. Displacement Thickness

The approximation used here for the boundary-layer thickness for the pipe was

$$\text{(flow area)} = \int_o^R \left(1 - \frac{U(r)}{U}\right) d(\text{perimeter area}) \qquad \text{(C12)}$$

where (see Fig. 2C)

$$\text{flow area} = 2\pi R\delta_1 - \pi\delta_1^2$$

$$\text{perimeter area} = 2\pi r dr$$

With a parabolic velocity distribution of,

$$\frac{U(r)}{U} = 1 - \frac{r^2}{R^2} \qquad \text{(C13)}$$

a displacement thickness expression was found to be

$$2R\delta_1 - \delta_1^2 = 2R \int_o^R \left(1 - \left(1 - \frac{r^2}{R^2}\right)\right) r dr \qquad \text{(C14)}$$

or,

$$2R\delta_1 - \delta_1^2 = R/2 \qquad \text{(C15)}$$

This expression resulted in a value of δ_1 of approximately (0.293)R.

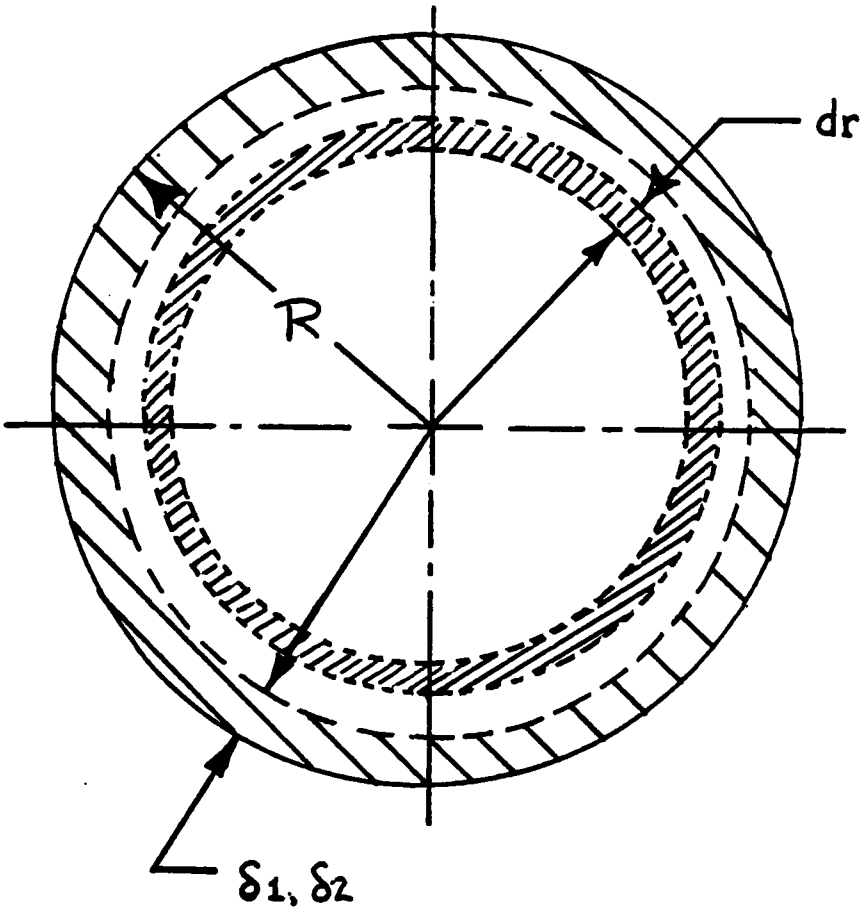

Fig C2 Pipe Flow Dimensions and Thicknesses.

2. Momentum Thickness

The boundary-layer momentum thickness was approximated using:

$$(2\pi R\delta_2 - \pi\delta_2^2) = \int_0^R \frac{U(r)}{U}\left(1 - \frac{U(r)}{U}\right)(2\pi r dr) \qquad (C16)$$

Substituting in Equation (C13) yielded

$$(2R\delta_2 - \delta_2^2) = \int_0^R \left(1 - \frac{r^2}{R^2}\right)\left(\frac{r^2}{R^2}\right) 4r dr \qquad (C17)$$

or,

$$2R\delta 2 - \delta_2^2 = \frac{R^2}{3}$$

which when solved for δ_2 yielded a value of $\delta 2 = (0.1835)R$.

Appendix D

Test Trials

The following computer program, written in its present form by J. Lawrence (Ref. 17), was used to test the prediction methods developed in this work. Table D shows the results of the runs made. The original function of this program was to investigate the effect of a pitching angle of attack on the flow parameters, Cl, Cd, etc. Here α was set at zero.

TABLE D

RL($X10^6$)	CL	TRIAL	
		R_1 = Const (X/1)	R = f(A) (X/1)
1.7	0.6	0.190	0.130
1.7	0.5	0.195	0.140
1.7	0.4	0.209	0.154
1.7	0.2	0.229	0.170
1.7	0.0	0.245	0.200
1.7	-0.2	0.270	0.217
5.0	0.4	0.100	0.124
5.0	0.2	0.108	0.135
5.0	0.0	0.124	0.174
5.0	-0.2	0.132	0.184

```
      PROGRAM POHL3
      COMPLEX CMPLX,EI,Z,DZETA,W
      OPEN (15,FILE='FLOWIN')
      REWIND 15
      OPEN (16,FILE='docout')
      EI=(0.,1.)
      RADIUS=1.131
      AMU=-.131
      READ (15,*,END=100) ALPHA,ADOT1,UINF
      ALPH1=ALPHA
      CON=3.1415927/180.
      THETA=180.
      TIME=0.0
      CALL DS(180.,RADIUS,CON,AMU,XLE,YLE)
      CALL DS(0.0,RADIUS,CON,AMU,XTE,YTE)
      XLE=ABS(XLE)
      CHORD=XLE+XTE
      PITCH=ADOT1*CON*0.5*CHORD/UINF
*
      K=100
      K1=K+1
      K2=(ALPHA+150)*100+K
*
      WRITE(16,30)UINF
      WRITE(16,40)ALPHA
      WRITE(16,50)ADOT1
      WRITE(16,52)
*
      ANGLE=ALPHA+THETA
      CALL U(ANGLE,RADIUS,CON,EI,UINF,AMU,ALPHA,U0)
      CALL DS(ANGLE,RADIUS,CON,AMU,X0,Y0)
      ANGLE=ANGLE-0.01
      CALL U(ANGLE,RADIUS,CON,EI,UINF,AMU,ALPHA,U1)
      CALL DS(ANGLE,RADIUS,CON,AMU,X1,Y1)
      ANGLE=ANGLE-0.01
      CALL U(ANGLE,RADIUS,CON,EI,UINF,AMU,ALPHA,U2)
      CALL DS(ANGLE,RADIUS,CON,AMU,X2,Y2)
      DS2=(SQRT((X2-X1)**2+(Y2-Y1)**2))/CHORD
      DS1=(SQRT((X1-X0)**2+(Y1-Y0)**2))/CHORD
*
*     Stagnation point velocity gradient computed using a
*     forward difference method; all other velocity gradients
*     computed using central difference method.
*
      DUDS=(U2-U0)/(DS1+DS2)
*
*     Second derivative of velocity computed using a
*     Taylor's Series expansion.
*
      D2UDS2=(U2-2.*U1+U0)/((DS1+DS2)/2.)**2
```

```
*
*       Enter initial boundary layer parameters.
*
        RLAMDA=7.052
        RK=0.0770
        FK=0.0
        DZDS=-0.0652*D2UDS2/(DUDS**2)
        ZZ=RK/DUDS
*
        N=50
        ANGLE=ALPHA+THETA-0.01
        XOC=(XO+XLE)/CHORD
        F2K=0.0
        WRITE(16,1)XOC,UO,F2K,RLAMDA,FK,RK,ZZ,DZDS
*
        ADOT=0.0
        DO 10 J=1,K
*
*       Function of this loop is to compute boundary layer
*       parameters at stagnation point, allowing the
*       boundary layer to steady-out before subjecting it
*       to a pitching airflow.
*
        N=N+1
*
*       Compute pertinent boundary layer parameters.
*
        ZZ=DZDS*DS1+ZZ
        RK=ZZ*DUDS
        FK=.47-6.*RK
        DZDS=FK/U1
*
        DELT=CHORD*DS1/U1
        TIME=TIME+DELT
        CALL U(ANGLE,RADIUS,CON,EI,UINF,AMU,ALPHA,U2)
        DUDT=(U2-U1)/DELT
        ANGLE=ANGLE-0.01
        ANGLE1=ANGLE-0.01
        CALL U(ANGLE1,RADIUS,CON,EI,UINF,AMU,ALPHA,U2)
        CALL DS(ANGLE1,RADIUS,CON,AMU,X2,Y2)
        ANGLEO=ANGLE+0.01
        CALL U(ANGLEO,RADIUS,CON,EI,UINF,AMU,ALPHA,UO)
        CALL DS(ANGLEO,RADIUS,CON,AMU,XO,YO)
        CALL U(ANGLE,RADIUS,CON,EI,UINF,AMU,ALPHA,U1)
        CALL DS(ANGLE,RADIUS,CON,AMU,X1,Y1)
        DS1=(SQRT((X1-XO)**2+(Y1-YO)**2))/CHORD
        DS2=(SQRT((X2-X1)**2+(Y2-Y1)**2))/CHORD
*
        DSS=DS1+DS2
        DUDS=(U2-UO)/DSS
        UDUDS=U1*DUDS
        XOC=(X1+XLE)/CHORD
```

```
      IF(N.LT.50) GO TO 10
      N=0
      WRITE(16,1)XOC,U1,F2K,RLAMDA,FK,RK,ZZ,DZDS
   10 CONTINUE
*
      ADOT=ADOT1
      N=0
      DO 20 J=K1,K2
*
*     Function of this loop is to compute the behavior
*     of the boundary layer as it is subjected to a
*     pitching airfoil.
*
      N=N+1
*
*     Compute the pertinent boundary layer parameters.
*
      ZZ=DZDS*DS1+ZZ
      RK=ZZ*(DUDS+DUDT/U1)
      CALL POHL(RK,RLAMDA)
      DEL2=37./315.-RLAMDA/945.-(RLAMDA**2)/9072.
      FK=2.*DEL2*(2.-.3683*RLAMDA+.0104*RLAMDA**2+
     + (RLAMDA**3)/4536)
      F2K=(.3-RLAMDA/120.)/DEL2
      DZDS=(FK+(4.+F2K)*ZZ*DUDT/U1)/U1
*
*     Compute the time increment for a particle to
*     travel from point (i) to point (i+1).
*
      DELT=CHORD*DS1/U1
      TIME=TIME+DELT
      DALPHA=DELT*ADOT
      ANGLE=ANGLE+DALPHA
      ALPH1=ALPH1+DALPHA
      CALL U(ANGLE,RADIUS,CON,EI,UINF,AMU,ALPH1,U2)
*
*     Compute the unsteady velocity gradient.
*
      DUDT=(U2-U1)/DELT
      ANGLE=ANGLE-0.01
      ANGLE1=ANGLE-0.01
      CALL U(ANGLE1,RADIUS,CON,EI,UINF,AMU,ALPH1,U2)
      CALL DS(ANGLE1,RADIUS,CON,AMU,X2,Y2)
      ANGLE0=ANGLE+0.01
      CALL U(ANGLE0,RADIUS,CON,EI,UINF,AMU,ALPH1,U0)
      CALL DS(ANGLE0,RADIUS,CON,AMU,X0,Y0)
      CALL U(ANGLE,RADIUS,CON,EI,UINF,AMU,ALPH1,U1)
      CALL DS(ANGLE,RADIUS,CON,AMU,X1,Y1)
*
*     Compute arc length and velocity gradient.
*
```

```
      DS1=(SQRT((X1-X0)**2+(Y1-Y0)**2))/CHORD
      DS2=(SQRT((X2-X1)**2+(Y2-Y1)**2))/CHORD
      DSS=DS1+DS2
      DUDS=(U2-U0)/DSS
      UDUDS=U1*DUDS
      XOC=(X1+XLE)/CHORD
C
C     Stop the computation at the quarter-chord.
C
      IF(XOC.GE.0.500) GO TO 25
      IF(N.LT.250) GO TO 20
      N=0
      WRITE(16,1)XOC,U1,F2K,RLAMDA,FK,RK,ZZ,DZDS
   20 CONTINUE
C
   25 WRITE(16,1)XOC,U1,F2K,RLAMDA,FK,RK,ZZ,DZDS
      WRITE(16,45)ALPH1
      WRITE(16,55)PITCH
      WRITE(16,60)RK
      WRITE(16,80)
      WRITE(16,81)TIME
    1 FORMAT(4X,F6.3,2(4X,F10.3),4X,F7.3,4X,F7.4,4X,F8.4,2(4X,E9.3))
   30 FORMAT(1H1,'BOUNDARY-LAYER PARAMETERS FOR ',F6.2,'FT/SEC'/)
   40 FORMAT(' INITIAL ANGLE OF ATTACK: ',F6.3,' DEGREES'/)
   45 FORMAT(/' FINAL ANGLE OF ATTACK: ',F6.3,' DEGREES'/)
   50 FORMAT(' PITCH RATE: ',F7.3,' DEGREES/SEC'/)
   52 FORMAT(6X,'XOC',10X,'U',11X,'F2K',9X,'LAMBDA',8X,'FK',
     + 9X,'RK',11X,'Z',11X,'DZDS'/)
   55 FORMAT(' PITCH PARAMETER: ',F7.5/)
   60 FORMAT(' K AT THE QUARTER-CHORD: ',F8.4/)
   80 FORMAT(' TIME TO REACH THE QUARTER-')
   81 FORMAT(' CHORD FROM THE STAGNATION POINT: ',F7.5,' SEC'/)
C
      STOP
  100 END


      SUBROUTINE U(ANGLE,RADIUS,CON,EI,UINF,AMU,ALPHA,UU)
      COMPLEX CMPLX,Z,EI,DZETA,W
C
      Function of this subroutine is to to compute the local
      value of velocity on a Joukowski Airfoil using complex
      potential flow theory.
C
      X=RADIUS*COS(ANGLE*CON)
      Y=RADIUS*SIN(ANGLE*CON)
      Z=CMPLX(X,Y)
      W=UINF*((1.,0.)-(RADIUS**2)/Z**2+
     + (2.*EI*RADIUS*SIN(ALPHA*CON))/Z)
      X=X+AMU
```

```
*
*       Z changed to represent values of coordinates used in
*       the transformation equation.
*
        Z=CMPLX(X,Y)
        DZETA=(Z**2-(RADIUS+AMU)**2)/Z**2
        UU=CABS(W)/CABS(DZETA)
        RETURN
        END
*
*
        SUBROUTINE DS(ANGLE,RADIUS,CON,AMU,X,Y)
        COMPLEX CMPLX,Z
*
*       Function of this subroutine is to compute the arc
*       length between two points on the Joukowski Airfoil.
*
        X=RADIUS*COS(ANGLE*CON)+AMU
        Y=RADIUS*SIN(ANGLE*CON)
        Z=CMPLX(X,Y)
        Z=Z+((RADIUS+AMU)**2)/Z
        X=REAL(Z)
        Y=AIMAG(Z)
        RETURN
        END
*
*
        SUBROUTINE POHL(RK,RLAMDA)
*
*       Function of this subroutine is to compute the value
*       of the separation parameter, Lamda, given a value
*       of K, as computed in the main program.
*
        RK1=-.160
        RK2=-.112
        RK3=0.00
        RK4=0.06
        RK5=0.076
        RK6=0.086
        RK7=0.0949
        IF(RK.LE.RK1) GO TO 10
        IF(RK.LE.RK2) GO TO 20
        IF(RK.LE.RK3) GO TO 30
        IF(RK.LE.RK4) GO TO 40
        IF(RK.LE.RK5) GO TO 50
        IF(RK.LE.RK6) GO TO 60
        IF(RK.GT.RK7) GO TO 70
*
        RLAMDA=.0149**2-(RK-0.08)**2
        RLAMDA=12.-100.*SQRT(RLAMDA)
        RETURN
```

```
*
   10     RLAMDA=(2./.012)*RK+14.0
          RETURN
*
   20     RLAMDA=(4./.044)*RK+2.18
          RETURN
*
   30     RLAMDA=(10./.14)*RK
          RETURN
*
   40     RLAMDA=83.33*RK
          RETURN
*
   50     RLAMDA=-1.9+115.*RK
          RETURN
*
   60     RLAMDA=-6.54+176.*RK
          RETURN
*
   70     RLAMDA=12.
          RETURN
          END
*
*
%
```

Bibliography

1. Schlichting, H.H. Boundary Layer Theory (Seventh Edition). New York: McGraw-Hill book Company, 1979.

2. Kays, W. W. and Crawford, M. E. Convective Heat and Mass Transfer. New York: McGraw-Hill Book Company, 1966.

3. Hunt, J. N. Incompressible Fluid Dynamics. New York: John wiley & Sons, Inc., 1964.

4. Lin, C. C. "On the Stability of Two-dimensional Parallel Flows Parts I, II, & III", Quarterly Journal of Applied Mathematics, Volume 3, Numbers 3 & 4: 1945 & January, 1946.

5. Verma, G. R. Hankey, W. L., and Scherr, S. J. "Stability Analysis of the Lower Branch Solutions for the Falkner-Skan Equations", AFFDL TR-79-3116: July, 1979.

6. Orzag, S. A. "An Accurate Solution of the Orr-Sommerfeld Stability Equation", Fluid Mechanics, Volume 50, Part 4: 1971.

7. van Ingen, J.L. "Theoretical and Experimental Investigations of Incompressible Boundary Layers With and Without Suction", Technological University Delft, Report VRH-124: October, 1965.

8. Schlichting, H. H., and Ulrich, A. "Zur Berechnung des Umschlages Laminar-Turbulent": Jb.Dt. Luftfahrt-Forschung, Volume I: 1940.

9. Davey, P. and Nguyen, H.P.F. "Finite-Amplitude Stability of Pipe Flow", Journal of Fluid Mechanics, Volume 45, Part 4: 1971.

10. Hodge, J. Class Notes for AE 8.27, "Turbulent Flow", School of Engineering, Air Force Institute of Technology, 1983.

11. Jumper, E.J. Private Communication. Air Force Institute of Technology, 1983.

12. Jaffe, N.A., Okamura, T.T., andSmith, A.M.O. "Determination of Spatial Amplification Factors and Their Application to Predicting Transition", AIAA Journal, Volume 8, Number 2: February, 1970.

13. Hall, D.J. and Gibbings, J.C., "Influence of Stream Turbulence and Pressure Gradient Upon Boundary Layer Transition", Journal of Mechanical Engineering Science. Volume 14: April, 1972.

14. Granville, P.S. "The Prediction of Transition from Laminar to Turbulent Flow in Boundary Layers on Bodies of Revolution", Naval Ship Research and Development Center, Bethesda, Maryland, Report 3900: September, 1974 (AD-787060).

15. Kao, T.W. and Park, C. "Experimental Investigations of the Stability of Channel Flows. Part 1. Flow of a Single Liquid in a Rectangular Channel, Journal of Fluid Mechanics, Volume 43, Part 1: 1970.

16. Crowder, H.J. and Dalton, C. "On the Stability of Poiseuille Flow in a Pipe", Journal of Computational Physics, Volume 7: 1971.

17. Lawrence, J. Private Communication. Air Force Institute of Technology, 1983.

18. Walz, A. Boundary Layers of Flow and Temperature. Cambridge: MIT Press, 1969.

19. Obremski, H.J., Morkovin, M.V., and Landahl, M. "A Portfolio of Stability Characteristics of Incompressible Boundary Layers", AGARDograph 134: March, 1969.

20. Hitchcock, J. Private Communication, Air Force Institute of Technology, 1983.

Vita

Richard D. Charles was born on 7 May, 1960, in Newark, Delaware. He graduated from Newark Senior High School in 1978 and entered Lehigh University in the same year. He graduated with a Bachelor of Science Degree in Mechanical Engineering and was commissioned into the United States Air Force Reserve in June, 1982. He then immediately entered the School of Engineering, Air Force Institute of Technology.

Permanent Address: 365 S. College Ave.
Newark, Del. 19711

UNCLASSIFIED

SECURITY CLASSIFICATION OF THIS PAGE

AD-A136 980

REPORT DOCUMENTATION PAGE

1a. REPORT SECURITY CLASSIFICATION: UNCLASSIFIED	1b. RESTRICTIVE MARKINGS
2a. SECURITY CLASSIFICATION AUTHORITY	3. DISTRIBUTION/AVAILABILITY OF REPORT: Approved for public release; distribution unlimited
2b. DECLASSIFICATION/DOWNGRADING SCHEDULE	
4. PERFORMING ORGANIZATION REPORT NUMBER(S): AFIT/GAE/AA/83D-4	5. MONITORING ORGANIZATION REPORT NUMBER(S)
6a. NAME OF PERFORMING ORGANIZATION: School of Engineering; 6b. OFFICE SYMBOL (If applicable): AFIT/EN	7a. NAME OF MONITORING ORGANIZATION
6c. ADDRESS (City, State and ZIP Code): Air Force Institute of Technology, Wright-Patterson AFB, Ohio 45433	7b. ADDRESS (City, State and ZIP Code)
8a. NAME OF FUNDING/SPONSORING ORGANIZATION; 8b. OFFICE SYMBOL (If applicable)	9. PROCUREMENT INSTRUMENT IDENTIFICATION NUMBER
8c. ADDRESS (City, State and ZIP Code)	10. SOURCE OF FUNDING NOS. — PROGRAM ELEMENT NO. / PROJECT NO. / TASK NO. / WORK UNIT NO.
11. TITLE (Include Security Classification): See Box 19	
12. PERSONAL AUTHOR(S): Richard D. Charles, B.S.M.E., 2d Lt, USAF	
13a. TYPE OF REPORT: MS Thesis; 13b. TIME COVERED: FROM _____ TO _____	14. DATE OF REPORT (Yr., Mo., Day): 1983 December; 15. PAGE COUNT: 73
16. SUPPLEMENTARY NOTATION	Approved for public release: IAW AFR 190-17. 3 JAN 1984 — Dean for Research and Professional Development, Air Force Institute of Technology (AIC), Wright-Patterson AFB OH (45433)
17. COSATI CODES: FIELD 20; GROUP 04; SUB. GR.	18. SUBJECT TERMS (Continue on reverse if necessary and identify by block number): Boundary Layer Transition, Flow Stability, Laminar Flow, Turbulent Flow, Reynolds Number

19. ABSTRACT (Continue on reverse if necessary and identify by block number)

Title: Predicting the Onset of Turbulence in the Presence of a Pressure Gradient

Thesis Chairman: Eric J. Jumper, Major, USAF

20. DISTRIBUTION/AVAILABILITY OF ABSTRACT: UNCLASSIFIED/UNLIMITED ☐ SAME AS RPT. ☐ DTIC USERS ☐	21. ABSTRACT SECURITY CLASSIFICATION: UNCLASSIFIED
22a. NAME OF RESPONSIBLE INDIVIDUAL: Eric J. Jumper, Major, USAF	22b. TELEPHONE NUMBER (Include Area Code): 513-255-3517; 22c. OFFICE SYMBOL: AFIT/ENY

DD FORM 1473, 83 APR — EDITION OF 1 JAN 73 IS OBSOLETE.

UNCLASSIFIED

SECURITY CLASSIFICATION OF THIS PAGE

An analytical study is presented regarding the determination of a pressure gradient dependent criterion for flow transition from laminar to turbulent flow. The results obtained were derived from two parallel approaches to flow stability; one of wave-dependent stability and the other of vorticity stability. In both cases, one of a variable transition Reynolds number dependent upon the ambient pressure gradient and the other one of a constant transition Reynolds number based on boundary-layer displacement thickness, the prediction results were either as good or better than those from available prediction methods. In addition these two criteria were used to predict transition locations on a NACA 0018 airfoil, again with favorable results.

END

FILMED

2-84

DTIC